

Organic Ices in Titan's Stratosphere

C.M. Anderson¹ · R.E. Samuelson^{1,2} · D. Nna-Mvondo^{1,3}

Received: 1 March 2018 / Accepted: 8 November 2018 / Published online: 26 November 2018
© The Author(s) 2018

Abstract Titan's stratospheric ice clouds are by far the most complex of any observed in the solar system, with over a dozen organic vapors condensing out to form a suite of pure and co-condensed ices, typically observed at high winter polar latitudes. Once these stratospheric ices are formed, they will diffuse throughout Titan's lower atmosphere and most will eventually precipitate to the surface, where they are expected to contribute to Titan's regolith.

Early and important contributions were first made by the InfraRed Interferometer Spectrometer (IRIS) on Voyager 1, followed by notable contributions from IRIS' successor, the Cassini Composite InfraRed Spectrometer (CIRS), and to a lesser extent, from Cassini's Visible and Infrared Mapping Spectrometer (VIMS) and the Imaging Science Subsystem (ISS) instruments. All three remote sensing instruments made new ice cloud discoveries, combined with monitoring the seasonal behaviors and time evolution throughout Cassini's 13-year mission tenure.

A significant advance by CIRS was the realization that co-condensing chemical compounds can account for many of the CIRS-observed stratospheric ice cloud spectral features, especially for some that were previously puzzling, even though some of the observed spectral features are still not well understood. Relevant laboratory transmission spectroscopy efforts began just after the Voyager encounters, and have accelerated in the last few years due

Ices in the Solar System
Edited by Nicolas Altobelli, Sebastian Besse and Claire Vallat

✉ C.M. Anderson
carrie.m.anderson@nasa.gov

R.E. Samuelson
robert.e.samuelson@nasa.gov

D. Nna-Mvondo
delphine.nnamvondo@nasa.gov

¹ NASA Goddard Space Flight Center, 8800 Greenbelt Road, Greenbelt, MD 20771, USA

² Department of Astronomy, University of Maryland College Park, 4296 Stadium Dr., College Park, MD 20742-2421, USA

³ University Space Research Association, 7178 Columbia Gateway Drive, Columbia, MD 21046, USA

to new experimental efforts aimed at simulating co-condensed ices in Titan's stratosphere. This review details the current state of knowledge regarding the organic ice clouds in Titan's stratosphere, with perspectives from both observational and experimental standpoints.

Keywords Ices · Clouds · Titan · Infrared spectroscopy · Infrared observations · Thermal infrared · Stratospheric composition

1 Setting the Stage

It comes as no surprise that ices thrive on the surfaces of many airless bodies in the outer solar system, *e.g.*, comets, gas and ice giant planet satellites, Kuiper Belt objects, etc. Ices are, however, also observed on solar system objects that, besides having discernible surfaces, also contain moderate atmospheres. We define this collection of objects to be the *terrestrial* group, with four primary members: Venus, Earth, Mars, and Saturn's moon Titan. Titan is naturally grouped with the other three terrestrial planets since it is more similar to Earth than dissimilar, despite Titan's distance of ~ 10 AU from the sun. Titan has an atmosphere that is about ten times more massive than Earth's, albeit Titan is less than half the size of Earth. Titan also has weather patterns with rain, clouds, and wind (see for example Porco et al. 2005; Roe et al. 2005; Rodriguez et al. 2011; Turtle et al. 2011a,b, and references therein), and even rivers, lakes, and seas (see for example Stofan et al. 2007; Hayes et al. 2008, 2011; Sotin et al. 2012; Hayes 2016, and references therein).

The four members of the terrestrial group have both similarities and differences. For example, the atmospheres of Venus and Mars are dominated by carbon dioxide (CO_2), and those of Earth and Titan are predominantly molecular nitrogen (N_2). Earth and Mars, however, are both fast rotators, resulting in latitudinal transport of heat and momentum preferentially through cyclonic-anticyclonic motion, whereas Venus and Titan are slow rotators, resulting in latitudinal transport of heat and momentum through cross-equatorial meridional circulation (Leovy and Pollack 1973; Flasar et al. 1981). On Titan, it is this slow atmospheric meridional circulation pattern that transports trace organic vapors from southern to northern latitudes in Titan's mesosphere and stratosphere, with a return flow of the atmospheric bulk in the troposphere from north to south (around northern winter solstice). The meridional flow pattern is expected to reverse near southern winter solstice, although observations of Titan's atmospheric vapors and temperatures have shown this reversal to occur a few years post equinox (see for example Teanby et al. 2012, 2017). For more information on Titan's general circulation patterns, see for example Hourdin et al. (2004), Lebonnois et al. (2012), Lora et al. (2015), Newman et al. (2016), and references therein.

Titan is much colder than Earth, with significantly more atmospheric CH_4 . A warmer Titan during its formation would have driven off volatiles like CH_4 , so Titan's lower temperature combined with its larger CH_4 abundance, helps to explain the important role of Titan's organic vapor inventory. The source of Titan's CH_4 vapor is the surface or subsurface, with a mole fraction of $\sim 1.5\%$ transported through Titan's cold trap, located at altitudes just below the tropopause, and on into the lower stratosphere. Assuming the CH_4 mole fraction remains constant above the cold trap, this mole fraction of 1.5% would also be present in the mesosphere and thermosphere. At these upper atmospheric altitudes, both CH_4 and N_2 are dissociated from solar UV photons and energetic particles originating from Saturn's magnetosphere, leading to complex organic chemistry (see Yung et al. 1984; Coates et al. 2009; Hörst 2017, and references therein). The resulting photofragments, atoms, and ions recombine into more exotic trace organic vapors, some of which are transported down to

the stratosphere to condense and form ice clouds (Maguire et al. 1981; Sagan and Thompson 1984; Frere et al. 1990; Samuelson et al. 1997; Samuelson et al. 2007; Coustenis et al. 1999; Raulin and Owen 2002; Anderson and Samuelson 2011; Anderson et al. 2014, 2016), while others in turn combine, polymerize, and form Titan's refractory aerosol particles (see Waite et al. 2004, 2007; Coates et al. 2009; Sciamma-O'Brien et al. 2010; Hörst 2017). Here we define *aerosol* as the refractory component of Titan's atmospheric particulate material (*i.e.*, haze), whereas the *stratospheric ices* are the volatile component of Titan's haze. These aerosol particles are very small, leading to relatively large absorption cross-sections at solar wavelengths, and small absorption cross-sections at thermal IR wavelengths (Tomasko 1980; Tomasko and Smith 1982; Rages and Pollack 1980; Rages et al. 1983; Tomasko et al. 2009; Doose et al. 2016). Thus, the aerosol particles are easy to heat and difficult to radiatively cool. Temperatures build up, and heat is transferred by conduction to adjacent vapor molecules. The aerosol particles exponentially attenuate the solar radiation, giving rise to an extensive stratosphere defined by the largest positive temperature gradient of any object in the solar system (Hanel et al. 2003), with a tropopause temperature on average of ~ 70 K (at ~ 42 km) and a stratopause temperature on average of ~ 190 K (at ~ 300 km) (Hanel et al. 1981; Flasar et al. 2005; Achterberg et al. 2008, 2011). Methane vapor also plays a non-negligible role in radiatively heating Titan's stratosphere.

From their formation altitudes, Titan's aerosol particles eventually drift downward into the stratosphere, providing heterogeneous nucleation sites for vapor condensation. It is condensation in Titan's stratosphere that is the ultimate sink mechanism for most of Titan's trace organic vapors. First, the Voyager 1 InfraRed Interferometer Spectrometer (IRIS; see Sect. 2), and later from its successor, the Cassini Composite InfraRed Spectrometer (CIRS; see Sect. 3), observed trace quantities of the hydrocarbon vapors ethane (C_2H_6), acetylene (C_2H_2), propane (C_3H_8), methylacetylene (C_3H_4), diacetylene (C_4H_2), and benzene (C_6H_6), and of the nitrile vapors hydrogen cyanide (HCN), cyanoacetylene (HC_3N), and cyanogen (C_2N_2) (see for example Hanel et al. 1981; Coustenis and Bezaud 1995; Samuelson et al. 1997; Coustenis et al. 1999, 2007, 2016, 2018; Teanby et al. 2007; Vinatier et al. 2010, 2015; Sylvestre et al. 2018), all capable of condensing to form ice clouds in Titan's cold mid to low stratosphere. The other three terrestrial atmospheres are incapable of generating such a diversity of trace organic vapors. Figure 1 gives an example showing the very rough approximate condensation altitudes for eight of Titan's stratospheric organic vapors during late southern fall at $79^\circ S$. The vapor abundances and temperature structure are determined from CIRS analyses during the Cassini flyby in July 2015. The saturation vapor pressure expressions for HC_3N , C_2N_2 , HCN, C_2H_2 , C_2H_6 , and C_6H_6 are taken from Fray and Schmitt (2009), while those for C_3H_4 and C_4H_2 come from Lara et al. (1996). For an overview on the evolution of Titan's stratospheric ice particles, see Sagan and Thompson (1984), Frere et al. (1990), Raulin and Owen (2002), Anderson et al. (2016).

For most of Titan's stratospheric organic trace vapors, CIRS-measured abundances and temperatures (see for example Coustenis et al. 2007, 2016, 2018; Teanby et al. 2007; Achterberg et al. 2008, 2011; Vinatier et al. 2010, 2015; Sylvestre et al. 2018) require condensation directly into the solid phase; the vapors will never condense directly to the liquid phase. Thus ice clouds, and never rain clouds, are always formed in Titan's stratosphere. As a generalization, the specific vapor compound and altitude location estimate of condensation depends on the vapor abundances and the temperatures at which saturation for each vapor occurs during its downward journey—cooling as it descends—through Titan's stratosphere. Once formed, these ice cloud particles will precipitate through the mid and lower regions of Titan's stratosphere, continually adding layers as they pass through altitude regions where the individual organic vapors successively become saturated. As the temperature continues to decrease

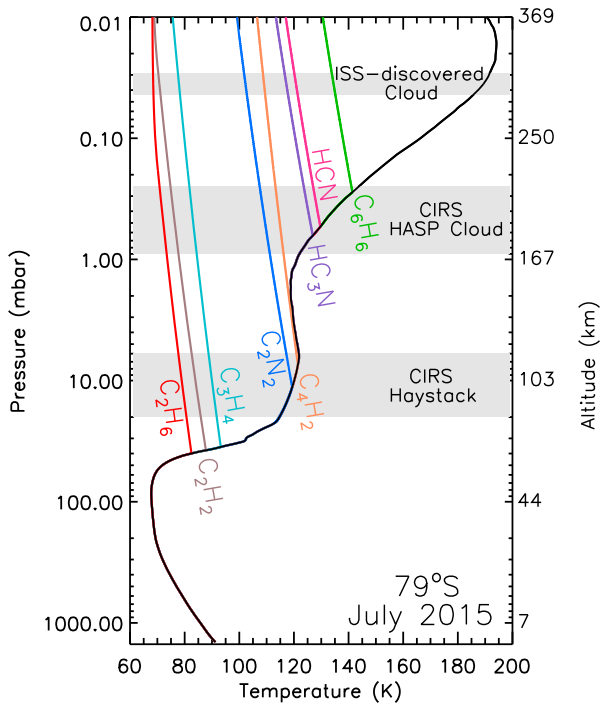


Fig. 1 Titan's pressure-temperature-altitude profile (black curve) at 79°S during late southern fall (July 2015). Superimposed are the vertical distributions for eight of Titan's stratospheric organic vapors (color-coded curves), showing the approximate altitude location for each individual vapor where condensation is possible—the intersections between the saturation vapor pressure curves and the temperature profile give a rough estimate of cloud top altitude. The vapor abundances and temperature structure are determined from CIRS analyses during the July 2015 Cassini flyby, and the saturation vapor pressures for HC_3N , C_2N_2 , HCN , C_2H_2 , C_2H_6 , and C_6H_6 are taken from Fray and Schmitt (2009), while those of C_3H_4 and C_4H_2 come from Lara et al. (1996). The gray color-coded rectangles represent the approximate altitude regions for three of Titan's observed stratospheric ice clouds: the upper rectangle indicates Titan's ISS-discovered south polar cloud (West et al. 2016), the middle rectangle depicts the CIRS-discovered High-Altitude South Polar (HASP) cloud, and the lower rectangle shows the CIRS Hoystack

with decreasing altitude, overlapping altitude regions will contain more than one condensing vapor at a time, leading to the onset of co-condensation (see for example Anderson and Samuelson 2011; Anderson et al. 2016, 2018). Co-condensation affects the developing physical structure of the ice particles being produced, and as laboratory experiments indicate (Anderson and Samuelson 2011; Anderson et al. 2016, 2018; Nna-Mvondo et al. 2018), considerably modifies the spectral characteristics from those of layered ices, most notably in the low energy part of the far-IR (see Anderson et al. 2018). Detailed examples for Titan ice analogs containing C_6H_6 , HCN , and/or C_2N_2 are given in Anderson et al. (2018), with an emphasis on the extensive modifications seen in the resulting co-condensed ice refractive indices and particle extinction cross sections for wavenumbers lower than $\sim 1000\text{ cm}^{-1}$ (wavelengths longer than $\sim 10\text{ }\mu\text{m}$).

Moreover, the resulting saturation vapor pressure for the combination of two or more vapors that undergo simultaneous condensation (*i.e.*, co-condensation) will be different than those of their individual compounds when considered separately. The condensation efficiency of Titan's stratospheric ices is much more complicated than typically considered,

and is a function of many parameters such as the ice and aerosol sticking coefficients, the binding energies of the different molecules, etc. (see for example Barth 2017, and references therein). Thus, the expected altitude of the co-condensed ice will be different than those of the individual compounds when considered separately. Phase diagrams representing the saturation levels of mixed vapors, rather than solely from their pure counterparts, remain to be determined.

As Titan's stratospheric ice particles continue to subside, they will eventually cross the tropopause and enter into the troposphere below, where some will disperse to lower latitudes due to atmospheric circulation and overall diffusion, and most will eventually sediment on to Titan's surface. The exceptions are ethylene (C_2H_4), which suffers from several strong photochemical sinks in Titan's lower stratosphere, thus reducing its mole fraction enough to inhibit vapor condensation, as well as the compounds CH_4 , C_2H_6 , and C_3H_8 , which will convert from the solid to liquid phase (melt) near and on Titan's surface. The majority of Titan's stratospheric organic ices will remain on the surface in the solid phase, and contribute—along with the aerosol—to the surface particulate inventory. Quantitative determinations of the relative abundance of these two organic particulates remain to be determined.

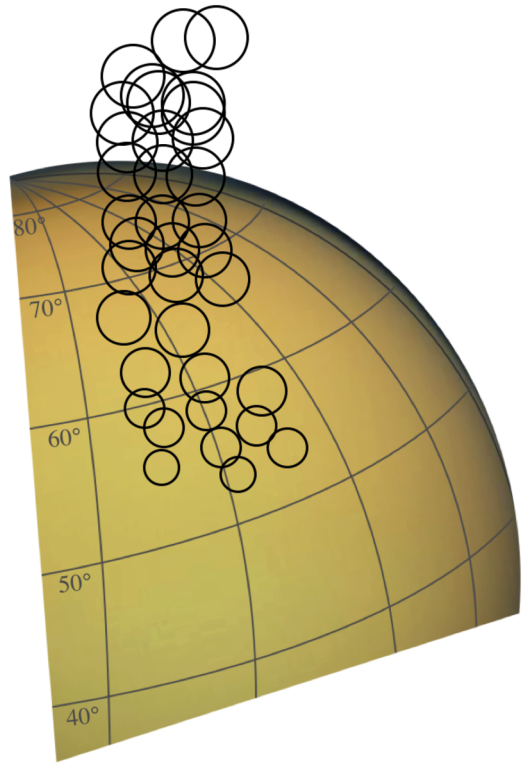
The remainder of this review is devoted to the observed vertical and latitudinal structure of Titan's stratospheric ice clouds as functions of season, their impact on Titan's atmosphere, and to their chemical identifications with the aid of laboratory thin ice film transmission spectroscopy. Some consideration of solid-state photochemistry as a stratospheric ice cloud formation mechanism will also be discussed.

2 The Pre-Cassini Era

In 1973, ground-based positive linear polarization white light measurements provided the first observational evidence that Titan had a scattering atmosphere due to clouds and/or aerosol particles (Veverka 1973). Six years later, the Pioneer 11 spacecraft flew by the Saturn system, returning the first high spatial resolution data of Titan's atmosphere. Although there were no cameras or spectrometers onboard, Pioneer 11 did contain a scanning photopolarimeter with red and blue broad band filters. Strong polarization near 90° phase angle—always unavailable from Earth—suggested that small particulates were suspended in Titan's atmosphere (Tomasko 1980; Tomasko and Smith 1982). One year later in 1980, Voyager 1 flew by the Saturn system, and using the onboard thermal IR spectrometer (IRIS), the organic molecules CH_4 , deuterated methane (CH_3D), C_2H_2 , C_2H_4 , C_2H_6 , C_3H_4 , C_3H_8 , C_4H_2 , C_2N_2 , HCN, HC_3N , as well as carbon dioxide (CO_2) and molecular hydrogen (H_2), were all detected in Titan's atmosphere (Hanel et al. 1981; Coustenis and Bezaud 1995; Samuelson et al. 1997; Coustenis et al. 1999). Excluding H_2 , which was seen in absorption (residing in the troposphere), all the remaining vapors were observed in emission (residing in the stratosphere), and analyses of these data indicated that most of the vapors were abundant enough to condense and form a profusion of organic ice clouds in Titan's cold mid to low stratosphere.

At this time, the possibility of organic ice clouds forming in Titan's stratosphere was unforeseen. The season on Titan was early northern spring, as Titan's north polar region had just emerged from winter, and it was fortuitous that IRIS was scheduled to perform a mosaic of Titan's north polar region—a spatially crude limb scan of the stratosphere—at high northern polar latitudes (see Fig. 2). The circles in Fig. 2 represent the 36-different tangent height positions of the IRIS fields-of-view (FOVs), which represents the FOVs footprint size on Titan's north polar limb. The FOV diameters range from roughly 220 km at the beginning

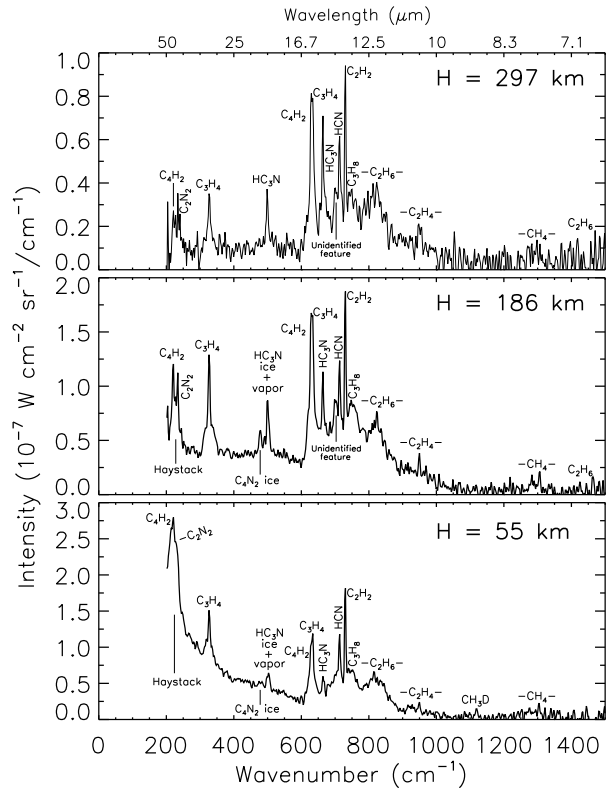
Fig. 2 Adapted from Samuelson et al. (1997). Schematic illustrating the Voyager 1 IRIS effective fields-of-view (FOVs) positioning on Titan's limb during the north polar mosaic observation recorded in November 1980. The black circles represent the 36-different limb positions of the effective IRIS FOV sizes. The 30-minute mosaic began high in Titan's stratosphere (top most circles) near 75°N when the spacecraft was furthest out from Titan, and then the FOV size steadily diminished, i.e., better spatial resolution on the limb, as the mosaic continued to sample deeper into Titan's stratosphere, and eventually onto the disk at the end of the mosaic (bottom most circles) near 55°N when the spacecraft was closest to Titan. Background Titan image credit: NASA/JPL-Caltech/Space Science Institute



of the observation (top most circles) to ~ 80 km near the end of the 30-minute observation (bottom most circles) (see Samuelson and Mayo 1991; Samuelson et al. 1997; Mayo and Samuelson 2005). The gradation in FOV size represents Voyager 1's relative distance from Titan—the spacecraft was further out at the beginning of the mosaic and closer to Titan at the end of the mosaic. Figure 3 shows some resulting limb spectra from this north polar limb mosaic at averaged tangent heights of 297 km, 186 km, and 55 km (each spectrum contains three averaged spectra), in which the original tangent height positions have been vertically-corrected by 65 km. Easily discernible are stratospheric emission signatures from the ν_6 band of HC_3N ice near 506 cm^{-1} , the ν_8 band of dicyanoacetylene (C_4N_2) ice at 478 cm^{-1} , and a spectrally broad and intense unidentified emission feature—presumed to be an ice cloud—that spectrally peaks at 221 cm^{-1} (see Samuelson et al. 1997; Coustenis et al. 1999; Mayo and Samuelson 2005). Over the last few decades, this latter spectral feature has been called by many names, such as the far-infrared cloud (Jennings et al. 2015), a polar condensate cloud (Jennings et al. 2015), the far-infrared 220 cm^{-1} cloud (Jennings et al. 2012a), the far-infrared haze (Jennings et al. 2012b), Haze B (de Kok et al. 2007), the $200\text{--}240\text{ cm}^{-1}$ feature (Samuelson et al. 1997), unidentified feature 2 (Coustenis et al. 1999), condensate X (Flasar and Achterberg 2009), and the Haystack (Anderson et al. 2014, 2018). Hereafter, we refer to Titan's unidentified 221 cm^{-1} stratospheric particulate feature as *the Haystack*. Had the IRIS mosaic instead occurred near Titan's south pole, the stratospheric ice detections in Titan's north polar region would have gone undiscovered, and the upcoming planning for the Cassini mission may have gone very differently for Titan.

Even though the ν_6 band of HC_3N ice near 506 cm^{-1} and its respective vapor at 499 cm^{-1} were observed as a single blended emission feature (see middle and lower panels in Fig. 3;

Fig. 3 Voyager 1 IRIS limb spectra recorded during the north polar limb mosaic in November 1980. Each of the three spectra, shown at tangent heights 297 km, 186 km, and 55 km, contain three averaged spectra. The tangents heights were vertically-corrected by 65 km from the original published values (Samuelson 1985, 1992; Coustenis et al. 1999; Mayo and Samuelson 2005) based on the observed continuum spectral dependences. Easily seen are stratospheric emission signatures from the vapors C_4H_2 , C_2N_2 , C_3H_4 , HC_3N , HCN , C_2H_2 , C_3H_8 , C_2H_6 , C_2H_4 , CH_3D , and CH_4 , as well as the ν_6 band of HC_3N ice near 506 cm^{-1} , the ν_8 band of C_4N_2 ice at 478 cm^{-1} , and a spectrally broad and intense unidentified emission feature that spectrally peaks at 221 cm^{-1} (see Samuelson et al. 1997; Coustenis et al. 1999; Mayo and Samuelson 2005). The latter spectral feature is called *the Haystack* (Anderson et al. 2014, 2018)



Samuelson 1985, 1992; Coustenis et al. 1999), a consequence of IRIS' fixed 4.3 cm^{-1} spectral resolution, the ice abundance relative to the gas was still observed to be more abundant in Titan's north polar lower stratosphere than at higher stratospheric altitudes (Samuelson 1985, 1992). This observed behavior in ice abundance is consistent with vapor condensation formation processes, in which HC_3N vapor forms higher up in Titan's atmosphere, cools as it diffuses/subsides downwards, and then condenses into ice cloud particles in Titan's cold, lower stratosphere.

IRIS also discovered the Haystack (Fig. 3), and observed it to behave similarly to that of HC_3N ice, appearing more abundant in Titan's lower stratosphere compared to those at higher stratospheric altitudes. The Haystack was presumed to be a stratospheric ice cloud due to 1) its spectrally broad and intense emission feature spanning wavenumbers 200 to 250 cm^{-1} , with a 221 cm^{-1} spectral peak, 2) its limited vertical dependence in Titan's north polar lower stratosphere, and 3) its restriction to latitudes poleward of $\sim 50^\circ N$ (see Samuelson 1985; Coustenis et al. 1999). Initial analyses of these data surmised the chemical composition of the Haystack was due to the $45\text{-}\mu\text{m}$ transverse optic vibration mode (Erickson et al. 1981) of water ice (Samuelson 1985; Coustenis et al. 1999). However, the water ice identification was eventually rejected given the amount of stratospheric water vapor calculated was three orders of magnitude below that of the IRIS-determined water ice upper limit (Yung et al. 1984; Samuelson 1985), as well as the obvious spectral mismatch between water ice and the Haystack (Samuelson 1985; Coustenis et al. 1999; Samuelson et al. 2007, see also Fig. 16). Subsequent laboratory thin ice film transmittance spectra were used to tentatively identify the chemical composition of the Haystack as crystalline propionitrile (C_2H_5CN)

(Khanna 2005). However, as discussed in Sect. 3.2.3 with the aid of Cassini CIRS spectra, pure C_2H_5CN ice was easily discounted as a likely Haystack candidate (see Fig. 16 and also Samuelson et al. 2007; Nna-Mvondo et al. 2018).

The ν_8 band of C_4N_2 ice at 478 cm^{-1} was also observed by Voyager 1 IRIS in Titan's north polar lower stratosphere (Khanna et al. 1987; Samuelson 1992; Samuelson et al. 1997; Coustenis et al. 1999); see middle and lower panels in Fig. 3. However, unlike with the observed behavior of HC_3N ice and its corresponding vapor, there was no observational evidence of C_4N_2 vapor in Titan's stratosphere. This was puzzling since the C_4N_2 vapor emission feature at 471 cm^{-1} would be easily detectable if C_4N_2 ice was condensing from the vapor to form the IRIS-observed ice clouds. The absent C_4N_2 vapor emission feature at 471 cm^{-1} led to a vapor mixing ratio upper limit calculation of 4×10^{-10} , and the C_4N_2 ice abundance was determined to be ~ 100 times greater than if the ice had condensed out from its uniformly-mixed vapor (Samuelson et al. 1997). C_4N_2 vapor is therefore not in equilibrium with the ice under the assumption that C_4N_2 ice clouds form as a result of vapor condensation, since both vapor and ice must be in equilibrium to maintain a steady-state. Here we define steady-state to only include the contribution from condensation in the absence of kinetics, since the latter is most likely a minor contributor to the steady-state of the stratospheric ice clouds in Titan's dense atmosphere. Photolytic decomposition of C_4N_2 vapor was later proposed to satisfy vapor-ice equilibrium (Samuelson et al. 1997). However, as discussed in Sect. 3.2.1, an alternate formation mechanism for C_4N_2 ice clouds was invoked 30-years later from analyses of CIRS far-IR spectra to explain this observed vapor-ice conundrum, while at the same time satisfying vapor-ice equilibrium (Anderson et al. 2016).

Continued analyses of Voyager 1 IRIS north polar limb far-IR spectra revealed the presence of a rather tenuous and uniformly-distributed ice cloud residing in Titan's lower stratosphere at altitudes between 58 and 90 km (Mayo and Samuelson 2005). These ice particles contributed to Titan's scattering continuum between $250\text{--}560\text{ cm}^{-1}$, with calculated effective particle radii between 1 and $5\text{ }\mu\text{m}$. Based on Mie calculation fits, the most likely candidates proposed for the chemical compositions were HCN ice and C_2H_6 ice, near the upper and lower boundaries of the cloud, respectively (Mayo and Samuelson 2005). However, from the spectral continuum analyses, no direct identifications of the chemical compositions were possible.

Lastly, an unidentified emission feature at 700 cm^{-1} was also observed—presumed to be an ice cloud—in Titan's northern polar stratosphere (see upper and middle panels in Fig. 3). C_3H_4 ice has been the only candidate proposed (Samuelson 1992; Coustenis et al. 1999). This feature was also observed 25 years later by CIRS in Titan's northern winter polar stratosphere (see Fig. 9); however, a definitive identification of this stratospheric ice feature still remains to be determined.

3 The Cassini Era

Nearly 25 years after the Voyager 1 flyby of Titan, the Cassini spacecraft entered into Saturn's orbit and began its remarkable 13-year journey through the Saturn system. During this time, Titan transitioned from northern to southern winter, and numerous stratospheric ice clouds comprising different chemical compositions were observed by three of Cassini's remote sensing instruments: the Visible and Infrared Mapping Spectrometer (VIMS), the Imaging Science Subsystem (ISS), and CIRS.

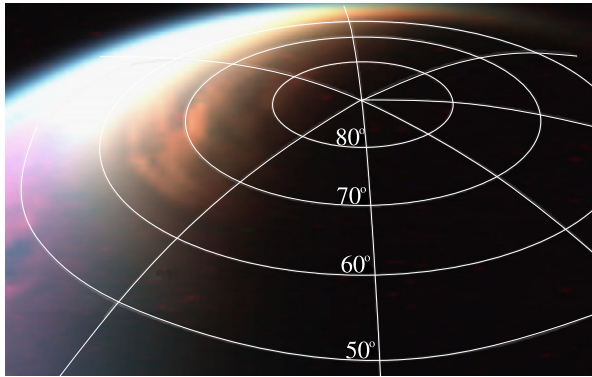


Fig. 4 Fig. 9 from Anderson et al. (2014); originally adapted from Le Mouélic et al. (2012). VIMS color composite image (red = 5 μm , green = 2.78 μm , and blue = 2.03 μm) of Titan's north polar winter cloud system observed in December 2006. Evident are two clouds morphologies—the homogeneously-distributed cloud extending poleward of $\sim 53^\circ\text{N}$ is most likely due to condensed ethane and the copper colored heterogeneously-distributed cloud most evident at 5 μm , seen poleward of $\sim 64^\circ\text{N}$, is most likely due to condensed methane

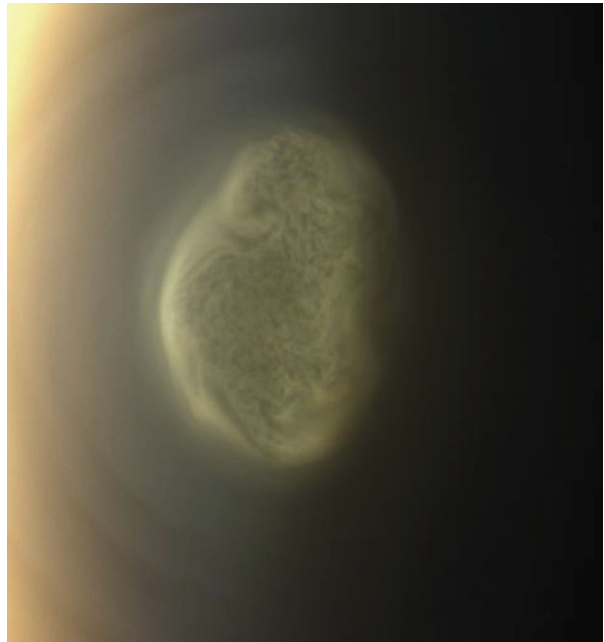
3.1 VIMS and ISS Observed Stratospheric Ice Clouds

Early on in the mission, VIMS detected diffuse and homogeneously-distributed ice clouds in Titan's north polar winter stratosphere, residing mostly at low stratospheric altitudes, spanning latitudes 51°N to 68°N (Griffith et al. 2006). Initially, between latitudes 48°N and 55°N , radiative transfer analyses were applied and clouds were inferred to reside between 30 and 60 km, with effective particle radii no larger than $\sim 3 \mu\text{m}$ (Griffith et al. 2006). The low altitudes ruled out clouds comprising chemical compositions other than C_2H_6 or CH_4 ice. Methane clouds, however, were ruled out due to the small particle size, the long-lasting and homogeneous cloud characteristics, along with a lack of opacity at 5 μm (see Fig. 4).

Subsequent VIMS observations of Titan's northern winter polar cloud revealed the emergence of a second cloud morphology with a heterogeneous horizontal structure poleward of $\sim 64^\circ\text{N}$; this was in addition to the homogeneously-distributed C_2H_6 ice clouds that appeared to diffusely extend to higher northern winter polar latitudes (see Fig. 4; Rannou et al. 2012; Le Mouélic et al. 2012). Concurrent CIRS observations, combined with Radio Science Subsystem (RSS) measurements, revealed Titan's tropopause temperatures at these high northern winter polar latitudes had cooled by several degrees below 70 K, suggesting CH_4 ice as the chemical composition of this second type of cloud morphology (Anderson et al. 2014). This second type of cloud was reported by Anderson et al. (2014) to form as a result of strong subsidence, and not convection, and were therefore named Titan's *Subsidence-Induced Methane Clouds (SIMCs)* (Anderson et al. 2014). Titan's SIMCs condense directly from the vapor to solid phase via subsidence, and at high northern winter polar latitudes in the very low stratosphere, these clouds were expected to form near 50 km at 85°N (in March 2005) and ~ 48 km at 74°N (in May 2007).

A more recent VIMS study detailed the time evolution of this northern winter polar cloud, and reported it to spatially cover the north polar region beginning at the onset of the mission in 2004 through spring equinox in 2009 (Le Mouélic et al. 2012, 2018). The investigators created VIMS mosaics orthographically re-projected over Titan's north pole, using an orange-reddish color to enhance the 4.78 μm spectral feature—this is most likely the ν_1 band of HCN ice (see Fig. 4 in Anderson et al. 2018). They also report the spectral feature at

Fig. 5 Image from the ISS narrow-angle camera depicting the ISS-discovered south polar cloud, acquired in June 2012. Cloud image scale is ~ 600 km across (see West et al. 2016). Image credit: NASA/JPL-Caltech/Space Science Institute



3.21 μm , which is most likely the ν_3 band of HCN ice (see Anderson et al. 2018). However, Le Mouélic et al. (2018) do not distinguish between the north polar cloud's differing cloud morphologies or their chemical compositions as discussed above; rather, focus remains on the 3.21 and 4.78 μm spectral features. The core of the cloudy structure is reported to begin thinning (becomes less opaque) between December 2007 and November 2008, with significant cloud dissipation most notable in March 2009. Finally, in June 2010, a small cloud residual was observed above Titan's fully illuminated north pole. This study did not provide any altitude information on this cloud system spanning the 2004 to 2009 time period since there was no radiative transfer modeling performed in this study.

Later on in Titan's mid southern fall season, the ISS instrument observed the rapid onset of a chemically-unknown particulate feature appearing at altitudes slightly below Titan's south polar stratopause (altitude location shown in Fig. 1; image shown in Fig. 5). This newly formed particulate feature was nominally observed by ISS at an altitude of 300 ± 10 km in May 2012, with its circulation pole located at 85.5°S , 263.7°W (West et al. 2016). Over the years, this upper stratospheric ice cloud feature has been referred to by many different names, such as the high-altitude southern polar cloud (de Kok et al. 2014), the south polar cloud (West et al. 2016), the winter polar vortex (Teanby et al. 2017), the vortex cloud (Jennings et al. 2017), the HCN ice cloud at Titan's south pole (Hörst 2017), and the southern polar vortex (Le Mouélic et al. 2018). In an effort to distinguish this distinct cloud from the many other observed stratospheric ice clouds, most notably those observed and discovered by CIRS, we hereafter call this cloud *the ISS-discovered south polar cloud*.

Despite the unusually high formation altitude of the ISS-discovered south polar cloud—slightly below Titan's stratopause—that was observed at altitudes typically too warm for ice cloud formation via vapor condensation (*i.e.*, vapors are sub-saturated at these high altitudes), the study by West et al. (2016) suggested that the unusual morphology and texture of this cloud seen in the ISS images was indeed characteristic of vapor condensation formation processes. ISS time monitoring of this cloud revealed its formation to have occurred as

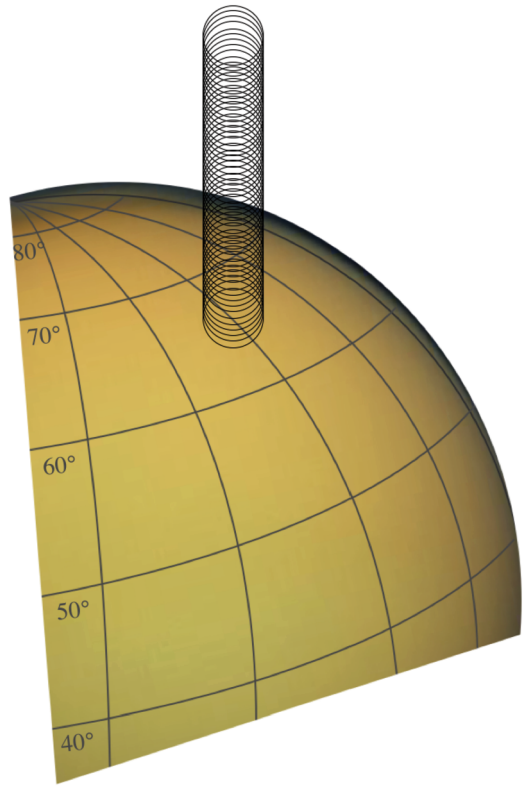
early as late 2011 (roughly two years post northern spring equinox), and visible in the ISS images up until late 2014 (West et al. 2016), depicting a rather long-lived and dynamically stable cloud—this implies relatively small ice particle radii. A recent VIMS study, however, monitored the time evolution of the ISS-discovered south polar cloud, revealing a significant increase in its spatial extent between 2012 and end of mission in 2017 (Le Mouélic et al. 2018). Specifically, the investigators report a spatial extension from 85°S down to 75°S in 2013, then down to 68°S in 2014, then further extending down to 60°S in mid-2016, and finally expanding down to ~58°S in April 2017. The complete south polar spatial extent still remains unknown since the south polar region became more engulfed in darkness as end of mission approached. However, the reported spatial expansion of the ISS-discovered south polar cloud is consistent with the horizontal growth of Titan's south polar vortex, reported to steadily increase in spatial extent from 90°S to 75°S in 2012 then down to 60°S in 2016 (Teanby et al. 2017).

The first identification of at least one of the chemical compounds contained within the ISS-discovered south polar cloud was reported by de Kok et al. (2014). These investigators analyzed a VIMS image cube acquired in June 2012 and identified the spectral feature at 3.21 μm to be that of HCN ice, with a derived ice cloud altitude of 300 ± 70 km, somewhat similar to the ISS-determined altitude location from May 2012 (West et al. 2016). Continued VIMS analyses between 2012 and 2017 identified both the HCN ice spectral signatures at 3.21 μm and 4.78 μm , and noted that these HCN ice spectral features were observed in most of the VIMS spectra spanning the 2012–2017 time period. This study, however, provided no information on the time-varying altitude locations of the ISS-discovered south polar cloud since the investigators did not perform any radiative transfer analyses. Thus, detailed analyses on the vertical extent of the time-varying ISS-discovered south polar cloud, its full chemical inventory, as well as its formation mechanism still remain to be determined.

3.2 CIRS-Observed Stratospheric Ice Clouds

Over the course of the Cassini mission, CIRS observed numerous ice clouds in Titan's stratosphere with varying chemical compositions such as HC_3N ice (Sect. 3.2.1, Anderson et al. 2010), C_4N_2 ice (Sect. 3.2.1, Anderson et al. 2016), co-condensed $\text{HC}_3\text{N}:\text{HCN}$ ice (Sect. 3.2.2, Anderson and Samuelson 2011), C_6H_6 ice (Sect. 3.2.5, Vinatier et al. 2018), co-condensed $\text{C}_6\text{H}_6:\text{HCN}$ ice (Sect. 3.2.4, Anderson et al. 2017), and the chemically-unidentified Haystack (Sect. 3.2.3, Samuelson et al. 2007, de Kok et al. 2007, Jennings et al. 2012a,b, 2015, Anderson et al. 2014, 2018). Most of these detections resulted from CIRS' expanded spectral range and higher spectral resolution over that of its predecessor IRIS, especially in the low energy part of the far-IR spectral region. IRIS had one interferometer, with the spectral range covering 200 to 1500 cm^{-1} (50 to 6.67 μm), and a fixed spectral resolution ($\Delta\nu$) of 4.3 cm^{-1} . CIRS, on the other hand, was comprised of two interferometers, had broader spectral coverage (10–1500 cm^{-1} ; 1000–6.67 μm), with variable spectral resolutions, although in practice, Titan spectra were recorded at $\Delta\nu = 14.1$ cm^{-1} , 2.56 cm^{-1} , and 0.48 cm^{-1} (all apodised FWHM values). One interferometer contained the mid-IR focal planes FP3 and FP4, spectrally covering 600–1100 cm^{-1} (16.67–9.09 μm) and 1100–1500 cm^{-1} (9.09–6.67 μm), respectively, while the second interferometer consisted of a single-element far-IR focal plane sensitive to the spectral range 10 to 600 cm^{-1} (1000 to 16.67 μm). The FP1 far-IR FOV was circular, with decreasing sensitivity from the center (at 0 mrad) to the edge, 3.2 mrad from the center, where the sensitivity dropped to zero (see Flasar et al. 2005; Anderson and Samuelson 2011). It is necessary to take the spatial FOV characteristics

Fig. 6 Conceptual CIRS far-IR limb scan of Titan's north polar region. The black circles represent the effective fields-of-view (FOVs) sizes of the CIRS far-IR detector (FP1). Altitude separation between contiguous FOVs is not drawn to scale. Typical CIRS limb scan durations were ~ 30 minutes, recording ~ 300 individual spectra at varying tangent heights, beginning near 350 km (top most circles) and then steadily sampling deeper into Titan's stratosphere, ending at tangent heights near -150 km (below the surface). There is a 98%–to–99% overlap of contiguous FOVs, enabling sub-FOV-diameter spatial resolution. Background Titan image credit: NASA/JPL-Caltech/Space Science Institute

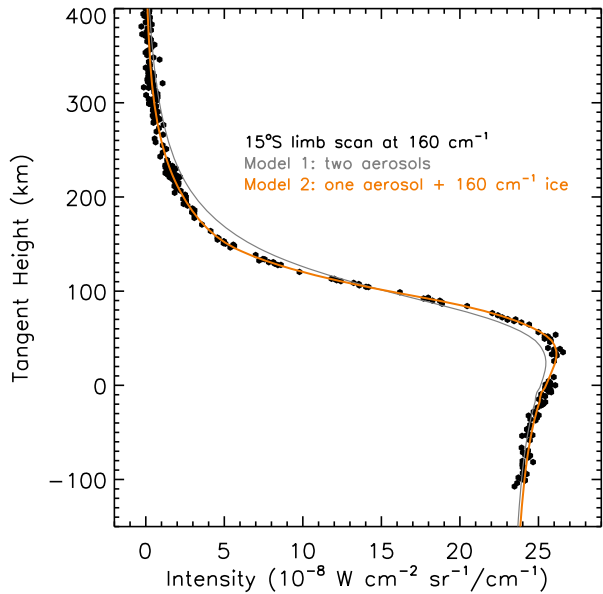


into account wherever data from the limb of Titan are being analyzed since spatial deconvolution in any radiative transfer model is essential. For a review of the CIRS instrument, see Flasar et al. (2005) and Jennings et al. (2017).

The vertical distributions and spectral dependences of the majority of the CIRS-observed stratospheric ice clouds were determined from analyses of CIRS far IR-targeted low spectral resolution limb scans. The black circles in Fig. 6 represent the placement of the CIRS far-IR FOV on Titan's limb during such a limb scan, and although not drawn to scale, are essentially contiguous footprints on Titan's limb that overlap the FOV by 98% to 99% at each tangent height. Each CIRS far-IR limb scan targeted ~ 300 individual tangent heights, beginning near Titan's lower mesosphere (~ 350 km) and then steadily sampling deeper into Titan's stratosphere, ending at tangent heights near -150 km, which is below Titan's solid surface horizon. The FOV diameter ranged from roughly 220 km at the beginning of the observations to ~ 100 km near the end of the 30-minute limb scan (see Anderson and Samuelson 2011). The significant overlap of contiguous FOVs enables a much narrower vertical resolution (~ 30 km) than FOV size would otherwise imply, and is optimized in the 100 to 250 cm^{-1} spectral region where the CIRS far-IR interferometer has the highest signal-to-noise ratio. Figure 7 gives a limb scan example at 15°S at 160 cm^{-1} acquired during northern winter in September 2006 and Fig. 8 gives a limb scan example at 75°S at 215 cm^{-1} acquired nine years later in late southern fall in July 2015.

The detailed procedure for determining sub-FOV-diameter spatial resolution is described in Anderson and Samuelson (2011). The vertical distributions for Titan's aerosol over three-to-four contiguous altitude regions (between 0 and 500 km), are each represented by ana-

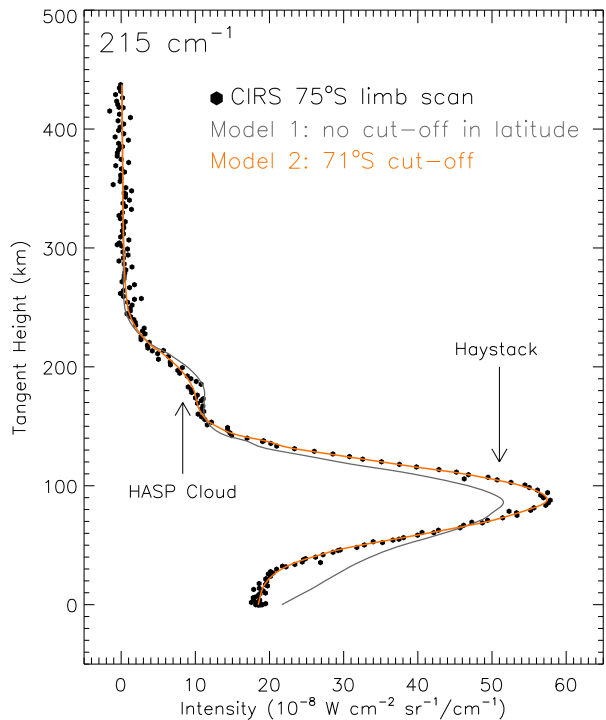
Fig. 7 CIRS far-IR limb-scan tangent height intensity profile at 15°S during northern winter in September 2006. Filled black hexagons represent the limb scan at 160 cm⁻¹—each symbol indicates a tangent height at which each spectrum was acquired. The solid gray curve is a radiative transfer model fit to the data assuming two vertically diffuse aerosol components with varying chemical compositions, while the solid orange curve represents a model fit with one aerosol component and the vertically restricted 160 cm⁻¹ ice cloud, which was found to reside at altitudes between 60 and 90 km at this latitude (Anderson and Samuelson 2011)



lytic solutions. Eventually the stratospheric ices are also included as an opacity source. The number of free parameters included in the separate analytic expressions for the different opacities are kept to a minimum. To determine the numerical values for the free parameters, the *Levenberg-Marquardt* nonlinear least squares fitting procedure is utilized. Anderson and Samuelson (2011) have empirically determined that the wavenumbers spanning ~ 100 to 250 cm⁻¹ have sufficient signal-to-noise ratios to determine accurate solutions. One reason the deconvolution of the intensity function (the average intensity over the FOV) works so effectively is because the 98–99% overlap in the CIRS FP1 FOVs during the far-IR limb scans essentially yields the derivative of the intensity function as well as the intensity function itself. This is true provided there is an adequate signal-to-noise ratio, which has been found in practice to occur at wavenumbers between ~ 100 and 250 cm⁻¹. For a detailed account of how the aerosol and stratospheric ice cloud vertical distributions are determined from CIRS far-IR limb scans, see Anderson and Samuelson (2011).

The extension of the CIRS far-IR spectral range down to 10 cm⁻¹ (1000 μm ; IRIS cut-off at 200 cm⁻¹ [50 μm]) opened up a previously unexplored far-IR spectral region containing a wealth of nitrile ice signatures, many of which are expected to comprise the chemical compositions of Titan's stratospheric ice clouds. The top panel in Fig. 9 shows a CIRS composite limb spectrum of Titan, with the FP1 FOV centered at a tangent height of ~ 125 km (mid-IR spectra are averaged over 100 to 150 km), recorded near 65°N during northern winter in 2006. In the bottom panel, the wavenumber dependence of the Planck intensity curve computed at 130 K is shown, which is comparable to the condensation temperatures in Titan's mid-to-low stratosphere. The Planck intensity is maximized in the low energy part of the far-IR at wavenumbers surrounding 200 cm⁻¹, coinciding with the spectral location for many nitrile ice cloud signatures (some hydrocarbons too) that reside at altitudes in Titan's mid to low stratosphere, and therefore contribute to the local environment there. On the other hand, the Planck intensities for wavenumbers higher than ~ 700 cm⁻¹ are much reduced at 130 K, indicating that these ice signatures will be much more difficult to detect in Titan's mid to low stratosphere. The strong vapor emission features seen in the upper panel for

Fig. 8 CIRS far-IR limb-scan tangent height intensity profile at 215 cm^{-1} during late southern fall in July 2015. Filled black hexagons represent the CIRS limb scan at 215 cm^{-1} , with each symbol representing a tangent height. Indicated in the figure are the altitude locations and intensity contributions from the HASP cloud and the Haystack. The gray curve shows a radiative transfer model fit that does not restrict the Haystack with latitude, resulting in a very poor fit. On the other hand, the orange curve represents a radiative transfer model fit that restricts the Haystack to latitudes poleward of $\sim 70^\circ\text{S}$, resulting in a very satisfactory fit. The Haystack, therefore, appears to be restricted to Titan's south polar high latitudes prior to the onset of Titan's southern winter season



wavenumbers higher than $\sim 700\text{ cm}^{-1}$ simply means that these vapors are originating and contributing to Titan's atmosphere at altitudes higher in the stratosphere than those of the ices. Thus, the low energy part of the far-IR is an ideal spectral location to detect Titan's mid to lower stratospheric ice clouds due to the combination of the Planck intensity maximizing, the spectral location of many low energy nitrile ice signatures, the CIRS high signal-to-noise ratio in this part of the spectrum, and the increase in stratospheric ice signal due to the observing geometry of the CIRS far-IR limb scans, *i.e.*, integrations along long path lengths of atmosphere. In order to determine the various ice cloud chemical compositions in Titan's stratosphere, as well as their formation mechanisms, the vertical distributions and spectral dependences of Titan's retrieved stratospheric particulate opacities must be combined with subsequent laboratory thin ice film transmission spectroscopy experiments. The remainder of this section details the various CIRS-observed stratospheric ice clouds.

3.2.1 HC_3N and C_4N_2 Ice Clouds

CIRS observed the ν_6 band of HC_3N ice at 506 cm^{-1} in Titan's lower stratosphere during three different seasons: northern winter, early northern spring, and late southern fall (Anderson et al. 2010, 2016). The ν_6 band of HC_3N ice at 506 cm^{-1} was easily separated from its corresponding gas at 499 cm^{-1} (unlike with IRIS) due to CIRS' higher spectral resolution. The upper left quadrant in Fig. 10 shows the first detection of the ν_6 band of HC_3N ice at 62°N during northern winter in July 2006, with the FPI FOV centered on a tangent height of 125 km (Anderson et al. 2010). The investigators (Anderson et al. 2010) reported a mean particle radius of $3.0 \pm 0.4\ \mu\text{m}$, an ice column abundance of $3.1 \times 10^{14}\text{ molecules cm}^{-2}$

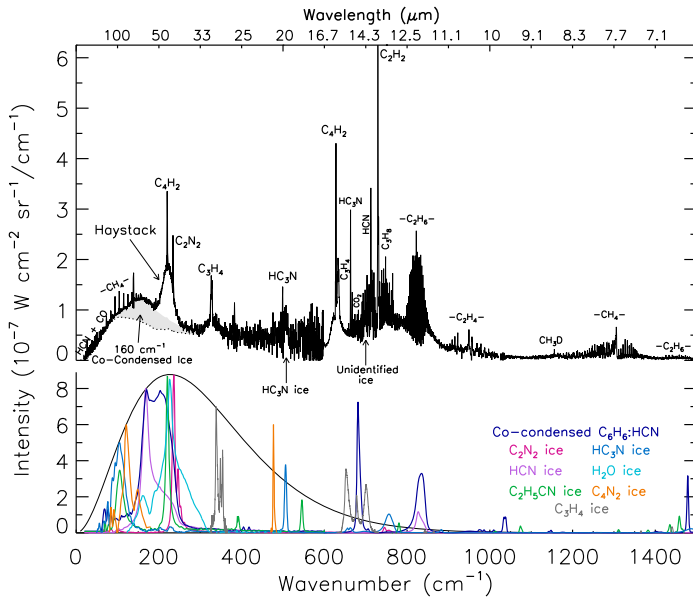


Fig. 9 Upper curve: CIRS far- and mid-IR limb spectra plotted as functions of wavenumber, recorded near 65°N during mid northern winter (July 2006) and averaged over tangent heights covering 100 to 150 km. Stratospheric organic vapors are labeled, as is the ν_6 band of HC_3N ice at 506 cm^{-1} , an unidentified ice feature at 700 cm^{-1} , the unidentified broad ice emission feature centered at 221 cm^{-1} (the Haystack), and the broad ice emission feature that peaks at 160 cm^{-1} , with its contribution to the continuum indicated by the light gray shaded region. Without the 160 cm^{-1} ice feature, the continuum would reduce to the dashed curve level. Lower curves: spectral dependences of laboratory-measured absorbances or imaginary part of the refractive index for various compounds that may contribute to ice clouds observed in Titan's stratosphere. The ices C_2N_2 , HCN, and co-condensed $\text{C}_6\text{H}_6:\text{HCN}$ (39% HCN, 61% C_6H_6) are taken from (Anderson et al. 2018), $\text{C}_2\text{H}_5\text{CN}$ from Nna-Mvondo et al. (2018), H_2O ice is taken from Hudson and Moore (1995), HC_3N ice comes from Moore et al. (2010), and C_4N_2 comes from Dello Russo and Khanna (1996). The Planck intensity curve computed at 130 K is superimposed (thin black curve), which is representative of the lower stratospheric temperatures at which ices are forming

(abundance value revised from Anderson et al. 2010), and a cloud top near 150 km. The upper right quadrant in Fig. 10 shows the second observation of HC_3N ice at 70°N in August 2007. This observation, however, recorded the ice emission features at two different tangent heights, with the FP1 FOV centered on 140 and 160 km, thus allowing for a vertical distribution determination of the HC_3N ice cloud (Anderson et al. 2010). A mean particle radius of $2.23 \pm 0.42\ \mu\text{m}$ and a corresponding column abundance of $2.7 \times 10^{14}\text{ molecules cm}^{-2}$ (abundance value revised from Anderson et al. 2010) were determined, with the cloud top residing at $\sim 165\text{ km}$. The best fit radiative transfer model found an HC_3N ice cloud thickness between ~ 10 and $\sim 20\text{ km}$. The limiting factors on cloud thickness and ice particle size are vapor abundance and large particle precipitation near the cloud bottom. The cloud thickness is consistent with calculations showing that about half of the HC_3N vapor is removed from the altitude where the cloud begins to condense (cloud top) at $\sim 4\text{ km}$ below the cloud top altitude. Moreover, the small HC_3N ice particle sizes are indicative of long-lived and dynamically-stable stratospheric ice clouds; large ice particles will precipitate out in relatively short times compared to that of the stable HC_3N ice clouds. The observed abundance

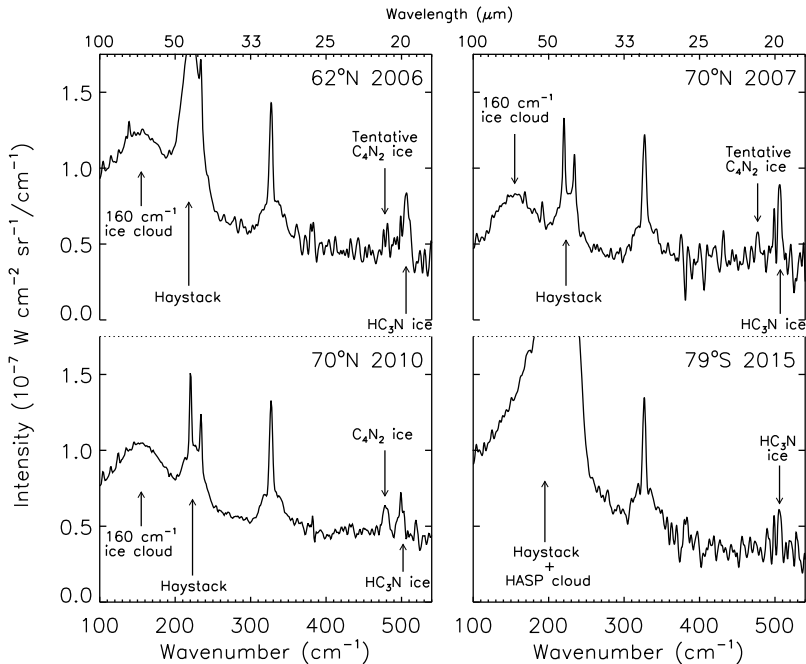
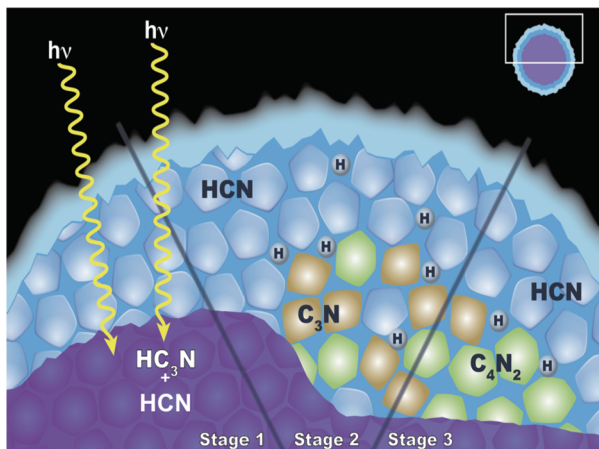


Fig. 10 CIRS limb spectra showing stratospheric HC_3N ice clouds, along with other stratospheric particulates, at three different Titan seasons. The upper left quadrant shows an average of 24 spectra, recorded at 62°N during northern winter (2006), with the FPI FOV centered at 125 km. Easily discernible are stratospheric particulate emission features from the 160 cm^{-1} ice cloud (Sect. 3.2.2), the Haystack (Sect. 3.2.3), a tentative detection of C_4N_2 ice, and the first detection of HC_3N ice (Anderson et al. 2010, 2014; Anderson and Samuelson 2011). The upper right quadrant shows an average of 25 spectra, recorded at 70°N during northern winter (2007), with the FPI FOV centered at ~ 150 km. The same stratospheric ice features are evident as those at 62°N (Anderson et al. 2010). The lower left quadrant shows an average of 254 spectra, acquired at $\Delta\nu = 2.56\text{ cm}^{-1}$, recorded at 70°N in early northern spring (2010), with averages over the FPI FOVs centered on 100 km, 150 km, and 200 km. Evident are stratospheric ice emission features from the 160 cm^{-1} ice cloud, the Haystack, HC_3N ice, albeit significantly reduced in abundance, and the first definitive detection of C_4N_2 ice (Anderson et al. 2016). The lower right quadrant shows an average of 35 spectra, recorded at 79°S during late southern fall (2015), with the FPI FOV centered on 125 km. At this time, there is no evidence of the 160 cm^{-1} ice cloud, and instead, the emergence of the HASP cloud is visible (Sect. 3.2.4), appearing at this tangent height as a broad shoulder to the left of the very strong Haystack. There is no trace of C_4N_2 ice, although the beginning of HC_3N ice cloud formation is observed (Sect. 3.2.1). The 2006, 2007, and 2015 spectra were recorded at $\Delta\nu = 0.48\text{ cm}^{-1}$, and shown here convolved with a gaussian kernel to $\Delta\nu = 2.56\text{ cm}^{-1}$

of HC_3N vapor at the cloud top, compared to that of the HC_3N ice abundance, is consistent with vapor condensation as the formation mechanism.

Following the first two HC_3N ice observations, a customized CIRS limb integration was designed to target a more precise vertical distribution and abundance determination of Titan's HC_3N ice clouds. In early northern spring (April 2010), CIRS recorded Titan limb spectra at 70°N at a spectral resolution of 2.56 cm^{-1} , with the FPI FOVs centered on tangent heights of 100 km, 150 km, and 200 km (Anderson et al. 2016). Each limb integration contained ~ 84 spectra, shown as a weighted average in the lower left quadrant in Fig. 10. However, the strength of the HC_3N ice emission feature at 506 cm^{-1} was significantly reduced compared to that observed during northern winter, and instead, the ν_8 band of C_4N_2

Fig. 11 Schematic illustrating an alternate C_4N_2 ice formation mechanism to that of vapor condensation. In this formation mechanism, photolysis within extant HCN and HC_3N ice particles has been proposed to form C_4N_2 ice—via solid-state chemistry (Anderson et al. 2016). In this case, only $\sim 1\%$ of C_4N_2 ice molecules will reside on the particle surface (in other words, unobservable), instead of 100% required by vapor condensation, thus satisfying vapor-ice equilibrium. For more details, see Anderson et al. (2016). Image credit: Jay Friedlander



ice at 478 cm^{-1} had emerged. Since both the C_4N_2 vapor emission features at 471 cm^{-1} and 107 cm^{-1} were absent, and with the rather large abundance of C_4N_2 ice observed, it was concluded that C_4N_2 vapor must be highly sub-saturated and therefore not in equilibrium with the pure ice—this unequivocally rules out vapor condensation as the formation mechanism. This observation was also the first indication that C_4N_2 ice formation may result from depletion of the HC_3N ice inventory, shedding some light on the formation mechanism of Titan's C_4N_2 stratospheric ice.

With C_4N_2 vapor observed by CIRS to be absent in Titan's stratosphere (this was also confirmed by Jolly et al. 2015), Anderson et al. (2016) postulated that solid-state photochemistry provides an alternate mechanism besides that of vapor condensation for producing Titan's observed C_4N_2 stratospheric ice clouds. In this scenario, HC_3N vapor subsides to condense at the initial cloud top. HCN vapor, being more than two orders of magnitude more abundant than HC_3N vapor (Coustenis et al. 2007, 2016), is also subsiding and soon afterwards, both HC_3N and HCN vapors enter into altitude regions where they undergo simultaneous saturation, *i.e.*, co-condensation. Once the two ices form a co-condensate, the individual molecules are very nearly in contact, so photochemistry is readily induced between the two molecules (see schematic in Fig. 11). On the other hand, if you only have a layered ice, then the HCN and HC_3N particles are close together only at their common boundary, so photochemistry is unable to promote interactions between the two ice layers very efficiently.

As detailed in Anderson et al. (2016), the UV irradiation initiates the solid-state photochemical reaction $HCN + HC_3N \rightarrow C_4N_2 + H_2$ within extant HC_3N :HCN co-condensed ice particles (see Fig. 11 and also Anderson et al. 2016, 2018). In order to inhibit diffusion of C_4N_2 molecules through the ice particle, the formation of an HCN ice barrier between the surface and interior of the particle is needed to keep the C_4N_2 ice in the interior, separate from the C_4N_2 vapor outside the particle. This is needed to maintain a low C_4N_2 vapor pressure in the presence of a relatively high C_4N_2 ice abundance buried deeper toward the center of the particle. Once all HC_3N ice is photolytically destroyed, the photochemical reaction will terminate. UV-irradiation studies of extant HCN: HC_3N co-condensed ices are still needed to confirm this formation mechanism.

Such a solid-state photochemical reaction has similarities to the terrestrial reaction $HCl + ClONO_2 \rightarrow HNO_3 + Cl_2$, which is known to produce HNO_3 coatings on water ice particles in Earth's stratosphere, a byproduct of the catalytic chlorine chemistry that produces

ozone holes in Earth's polar stratosphere (see for example Molina et al. 1987; Solomon 1999). The cold temperatures in Titan's lower stratosphere combined with the associated strong circumpolar winds that isolate polar air act in much the same way as on Earth, giving rise to compositional anomalies and stratospheric condensate clouds that are the sites of heterogeneous chemistry. While there are differences in detail—the terrestrial case entails oxygen and halogen compounds, whereas Titan's chemistry involves organics—the overall picture is remarkably similar on the two worlds.

The final CIRS observation revealing the ν_6 band of HC_3N ice in Titan's stratosphere was discovered at 79°S in late southern fall (July 2015), following the observed reversal of the meridional circulation pattern (see for example Teanby et al. 2012, 2017). The lower right quadrant in Fig. 10 shows the resulting limb integration spectrum, with the CIRS far-IR FOV centered on a tangent height of 125 km. This limb integration shows the emergence of stratospheric HC_3N ice as Titan's south polar region was heading into winter; particle size and abundance are currently being determined.

3.2.2 The 160 cm^{-1} Ice Clouds

The 160 cm^{-1} ice cloud is the name given to a spectrally broad ($\sim 100\text{--}300\text{ cm}^{-1}$), quasi-continuum ice emission feature, spectrally peaking at 160 cm^{-1} , located in Titan's northern winter lower stratosphere (Anderson and Samuelson 2011; Anderson et al. 2014, 2018, see Figs. 9, 10, 12). Its significant contribution to Titan's continuum is shown by the gray shaded region in the upper panel in Fig. 9 and also evident in Fig. 10. This ice cloud was discovered using the CIRS low spectral resolution far-IR limb scans (Fig. 7; Anderson and Samuelson 2011), which enable separation of Titan's vertically-restricted stratospheric ice clouds from the surrounding ubiquitous aerosol continuum. As discussed in Sect. 3.2, the significant overlap in FOVs during a CIRS far-IR limb scan allows for not only the average intensity over each FOV but also the derivative of these intensities (at wavenumbers where there is sufficiently high signal-to-noise ratios), enabling a sub-FOV-diameter vertical resolution. Figure 7 gives an example of such a limb scan at 160 cm^{-1} , recorded during the northern winter season in September 2006 at 15°S . Specifically, the figure shows the tangent height-intensity profile containing ~ 300 individual limb spectra (solid black hexagons), with the FOV center—for each tangent height observation—separated by a few km at most. It became clear very early in the analysis that the limb scans spanning wavenumbers $\sim 100\text{--}300\text{ cm}^{-1}$ required an additional, vertically-limited, opacity source to that of the ubiquitous aerosol in order to better fit the CIRS limb scan observations. The gray curve in Fig. 7 shows the best fit radiative transfer model at 160 cm^{-1} consisting of two vertically diffuse aerosols with different chemical compositions. It is clear that the fit is rather poor, and instead, when one aerosol and one vertically restricted stratospheric ice cloud—the latter residing at altitudes between ~ 60 and 90 km in the lower stratosphere—are included, the fit dramatically improves, as shown by the orange curve (Anderson and Samuelson 2011). The 160 cm^{-1} ice cloud was found by Anderson and Samuelson (2011) to be a geometrically thin and effectively continuous sheet of ice cloud that tends to increase monotonically from roughly 60°S to high northern polar latitudes during northern winter. The 160 cm^{-1} ice cloud's derived spectral dependence at 15°S is shown by the black curve in Fig. 12. From the radiative transfer analysis along with predicted cloud top locations for the various organic vapors in Titan's stratosphere, this cloud was expected to contain both HCN and HC_3N ice due to its altitude location in Titan's lower stratosphere.

The 160 cm^{-1} ice emission feature is located in a spectral region that contains overlapping, low-energy lattice vibration features (librations) of multiple nitrile ices (see bottom

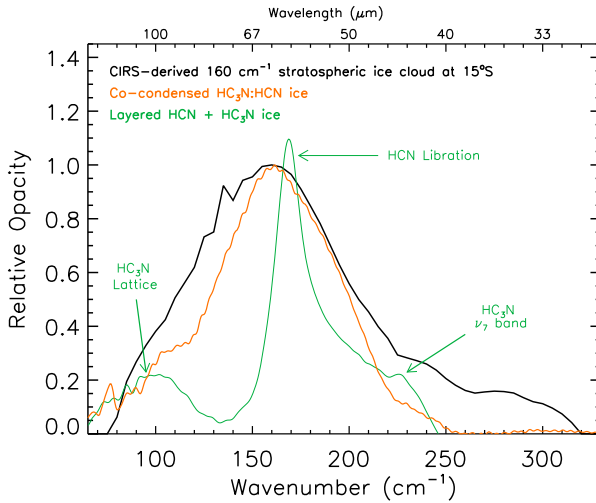


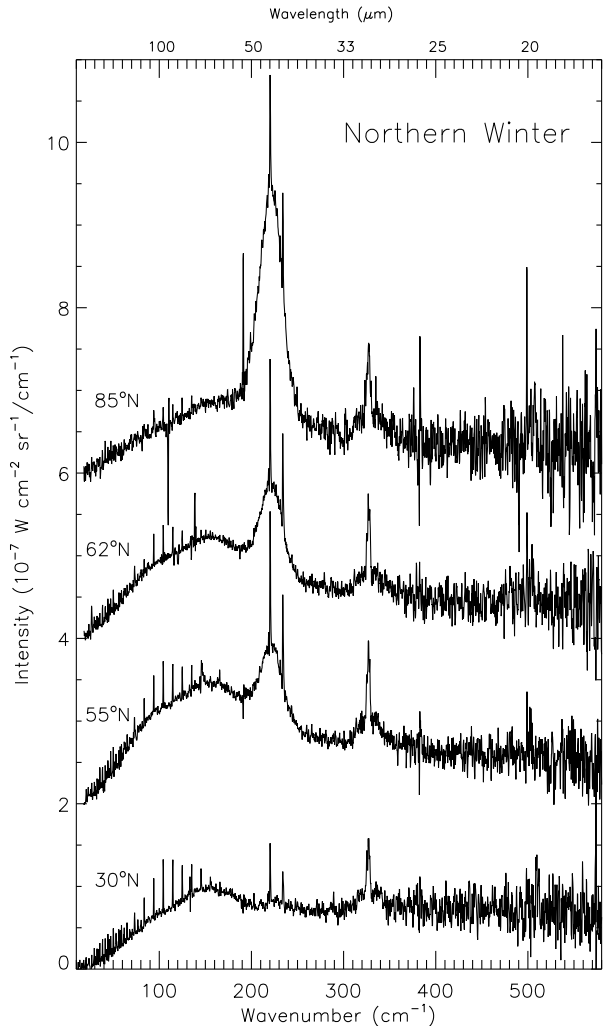
Fig. 12 Modified from Anderson and Samuelson (2011) and Anderson et al. (2018). Black curve represents the CIRS-derived spectral dependence of Titan's 160 cm^{-1} ice cloud discovered at lower stratospheric altitudes (~ 60 to 90 km) during northern winter at 15°S . The green curve shows the weighted sum of individual HCN and HC_3N ices from thin ice film transmission spectroscopy (vapors deposited at 30 K ; see also Moore et al. 2010). As discussed in Anderson et al. (2018), in the low-energy part of the far-IR, the sum of the individual ices is nearly identical to layered ice experiments. The orange curve depicts a co-condensed thin ice film containing mixed HC_3N and HCN, demonstrating that co-deposition (*i.e.*, co-condensation) experiments better reproduce the CIRS observations

panel in Fig. 9 and also Fig. 16), and as laboratory experiments indicate (Anderson and Samuelson 2011; Anderson et al. 2018), is consistent with an ice mixture dominated by HCN and HC_3N ice formed via co-condensation processes in Titan's stratosphere (Anderson and Samuelson 2011; Anderson et al. 2014, 2018). Thin ice film transmission spectroscopy reveals that layered HC_3N and HCN ices do not reproduce the 160 cm^{-1} ice cloud feature; rather, the ice cloud is consistent with ice particles formed via co-condensed HC_3N :HCN (see Fig. 12; Anderson and Samuelson 2011, Anderson et al. 2018), resulting from combinations of the ν_7 band and lattice modes of HC_3N and the libration mode of HCN (Anderson and Samuelson 2011; Anderson et al. 2018).

3.2.3 The Haystack

As discussed in Sect. 2, the Haystack is a name given to one of Titan's long-lived stratospheric ice clouds with an unknown chemical composition (Anderson et al. 2014, 2018). The Haystack is easily identifiable due to its broad emission feature spectrally peaking at 221 cm^{-1} , and spanning wavenumbers ~ 200 – 250 cm^{-1} (see Figs. 9, 13, 14, 15). The Haystack's spectral signature is quite strong, suggesting that whatever it is made out of is very abundant. The large spectral extent and its spectral location in the far-IR further suggests that the Haystack contains more than one chemical compound. Some chemical compounds that have been proposed as the identity of the Haystack are water ice (Samuelson 1985; Coustenis et al. 1999), crystalline $\text{C}_2\text{H}_5\text{CN}$ (Khanna 2005), predominantly pure HCN ice (de Kok et al. 2008), and complex nitriles that have $-\text{C}-\text{CN}$ bending vibrations (Jennings et al. 2012a,b).

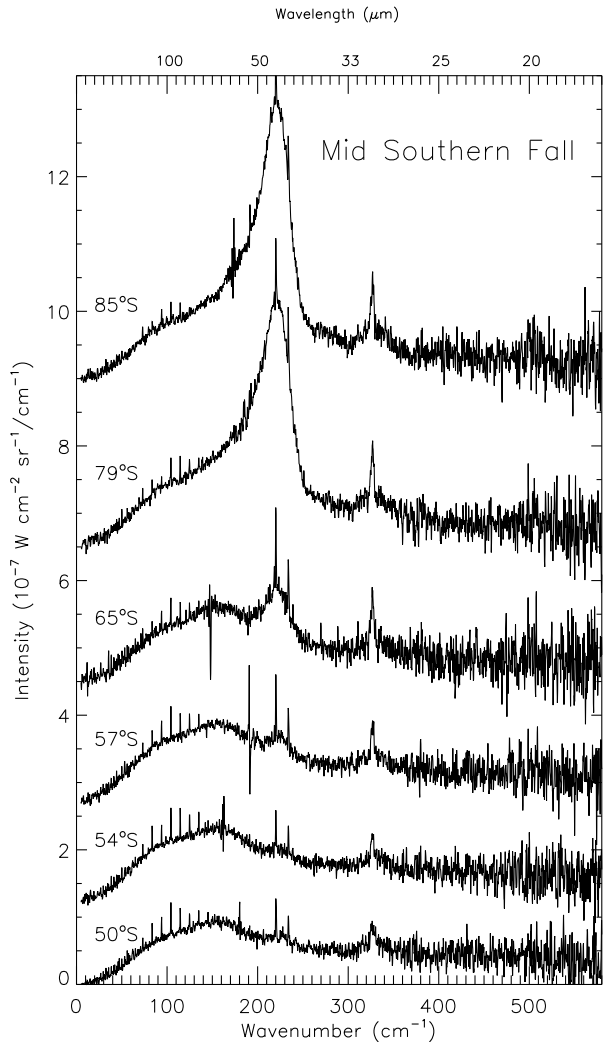
Fig. 13 CIRS far-IR limb integrations spanning 30°N to 85°N during northern winter, all acquired at tangent heights of ~125 km. The 85°N, 62°N, 55°N, and 30°N spectra were recorded in early 2005, mid 2006, early 2006, and late 2006, respectively. The spectra at 55°N, 62°N, and 85°N were vertically offset from the 30°N spectrum. With the exception at 30°N, the Haystack is evident at the remaining latitudes, with its strongest signature near the north pole



As discussed above in Sect. 2, the Haystack was first observed by Voyager 1 IRIS in Titan's early northern spring stratosphere (November 1980) at latitudes poleward of ~50°N (Samuelson 1985; Coustenis et al. 1999) (Fig. 3). Later, with Cassini CIRS, the Haystack was first observed at the beginning of the mission in 2004 (mid northern winter), and then continuously observed at high northern polar latitudes throughout northern winter (see Fig. 13), and well into northern spring (Samuelson et al. 2007; de Kok et al. 2007; Jennings et al. 2012b; Anderson et al. 2014). As with IRIS, the Haystack appeared to be restricted to latitudes poleward of ~50°N during northern winter. A few years later during mid southern fall, the Haystack made its debut at high southern polar latitudes (Figs. 10, 14, 15; Jennings et al. 2012a, 2015), and was observable in CIRS far-IR disk-viewing spectra up until end of mission (data were acquired through May 2017).

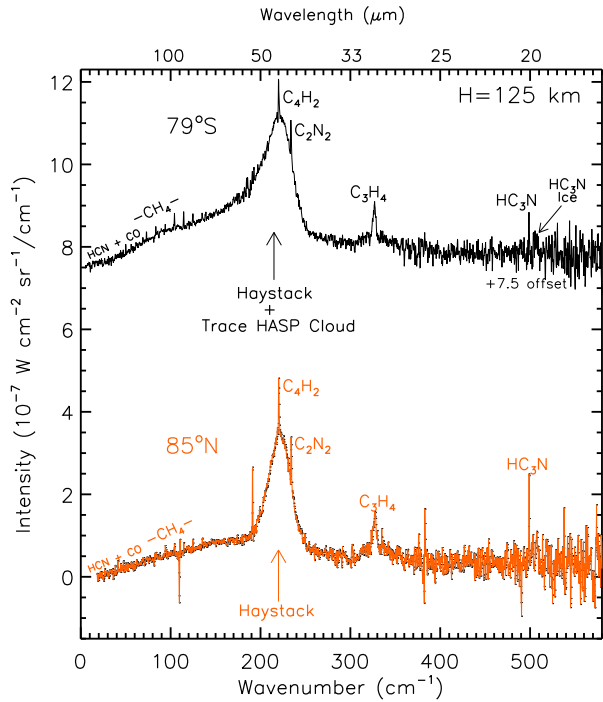
Figure 16 shows a CIRS far-IR limb integration averaged spectrum ($\Delta\nu = 0.48 \text{ cm}^{-1}$) recorded at 85°N at a tangent height of ~135 km during mid northern winter in March 2005. This figure shows the very strong emission feature of the Haystack (solid black curve), ob-

Fig. 14 CIRS far-IR limb integrations spanning 50°S to 85°S during late southern fall, all recorded at tangent heights of ~125 km. The spectra were recorded in late 2015 (85°S), mid 2015 (79°S), early 2016 (65°S and 57°S), and mid 2016 (54°S and 50°S). The spectra at 54°S, 57°S, 65°S, 79°S, and 85°S were vertically offset from the 50°S spectrum



served when it was at its strongest during northern winter. The varying color-coded continuum intensity curves were generated from Mie scattering calculations (for a 2 μm particle radius), coupled with our radiative transfer model (model detailed in Anderson and Samuelson 2011), using the appropriate aerosol and collision induced absorption (CIA) opacities and the temperature structure at 85°N (see Anderson et al. 2014). The optical constants for H_2O ice (aqua curve) were taken from Hudson and Moore (1995); vapor was deposited at 140 K, $\text{C}_2\text{H}_5\text{CN}$ ice (orange curve) were taken from Nna-Mvondo et al. (2018); vapor was deposited at 135 K, HCN ice (green curve) were taken from Anderson et al. (2018); vapor was deposited at 110 K, co-condensed $\text{C}_6\text{H}_6:\text{HCN}$ ice (purple curve) containing a 4:1 mixing ratio were taken from Anderson et al. (2017); vapor was deposited at 110 K, and co-condensed $\text{C}_6\text{H}_6:\text{C}_2\text{H}_5\text{CN}:\text{HCN}$ ice (pink curve) containing a 3.6:1.4:1.0 mixture ratio were determined from Nna-Mvondo et al. (2018); vapor mixture was deposited at 110 K. The obvious spectral mismatch between the Haystack and all five ice examples is evident.

Fig. 15 CIRS far-IR limb integrations recorded at 79°S in late southern fall (black curve; July 2015) and at 85°N in mid northern winter (orange curve; March 2005), with the FP1 FOV centered on ~125 km. Noticeable immediately is the appearance of a spectral mismatch between the Haystack at 79°S compared to the Haystack at 85°N. The Haystack's spectral dependence is actually unaltered. Instead, the broad shoulder comprising the lefthand side of the Haystack at 79°S is due to the HASP cloud, appearing to spectrally pollute the Haystack. The observed spectral pollutions result from the large range in stratospheric altitudes averaged over the FP1 FOV during the limb integrations. The HASP cloud and the Haystack are separated vertically by ~100 km at 79°S, determined from CIRS data analyses of low spectral resolution far-IR limb scans (see Sect. 3, Fig. 8)



Specifically, for pure C_2H_5CN ice, it was ruled out as a likely Haystack compound due to its very strong low-energy lattice mode (Samuelson et al. 2007). However, as seen in the figure, this lattice mode is easily damped out when C_2H_5CN ice becomes part of a co-condensed ice. This is expanded on in Nna-Mvondo et al. (2018). C_2H_5CN ice may still indeed contribute to the Haystack's identity, as part of a co-condensate, although the formation mechanism will most likely be something other than vapor condensation. This quashing trend of low-energy ice modes is also evident with the strong libration mode of HCN ice. The libration mode of pure HCN ice spectrally peaks near 168 cm^{-1} , but when co-condensed with C_6H_6 ice (purple curve) or co-condensed with C_6H_6 and C_2H_5CN ice (pink curve), the libration mode of HCN is easily modified. A detailed discussion on co-condensed ices, as they specifically pertain to Titan's stratospheric ices, are found in Anderson et al. (2018).

The first detection of the Haystack in Titan's south polar stratosphere occurred in the mid southern fall season (July 2012; Jennings et al. 2012a). The investigators used CIRS weighted-averaged disk-viewing spectra—targeting 75°S—recorded at Cassini-Titan distances $>50,000\text{ km}$. This larger distance from Titan results in a larger FP1 FOV diameter size ($\sim 320\text{ km}$), in which the FOV subtended both Titan's limb and disk. Such an observation was unavoidable, however, since Cassini's orbit at this time was in an inclined orientation so the dedicated far-IR limb scans required to constrain the vertical and latitudinal distributions (discussed in Sect. 3.2) at high polar latitudes were not possible. Thus, the limitations imposed by this type of disk-viewing observation prevents detailed vertical and latitudinal information. However, radiative transfer analyses could still improve the current state of knowledge especially at this critical moment in time when CIRS serendipitously caught the onset of the Haystack's formation.

By July 2015, Cassini had returned to a lower inclination, allowing for far-IR limb-viewing of Titan's south polar stratospheric regions, recorded at distances between $\sim 15,000$

and 35,000 km off Titan's limb. CIRS FP1 high spectral resolution limb integrations (typically centered on 125 km tangent height) at multiple latitudes during Titan's late southern fall season are shown in Fig. 14. Although this figure depicts a strong latitudinal dependence of the Haystack, in limb integration mode (or sit-and-stare mode), the large CIRS FP1 FOV collects and integrates the signal from many altitudes simultaneously. This causes the Haystack's spectral signature to appear in lower latitude spectra, where the Haystack actually does not reside. From analysis of far-IR limb scans acquired in July 2015 (example limb scan at 215 cm^{-1} is shown in Fig. 8), our best fit radiative model (model details given in Anderson and Samuelson 2011) reveals the Haystack to reside at latitudes poleward of $\sim 70^\circ\text{S}$. This point is further illustrated at 215 cm^{-1} in Fig. 8. When no attempt is made to restrict the Haystack with latitude, the resulting fit is very poor (gray curve). However, when the presence of the Haystack is restricted to latitudes poleward of $\sim 70^\circ\text{S}$, a very satisfactory fit (orange curve) results. From these analyses, the Haystack's altitude location is found to reside fairly deep in Titan's stratosphere, with a cloud top near ~ 110 km. This is evident in the limb scan at 215 cm^{-1} (Fig. 8) and also indicated in Fig. 1.

Observations of the Haystack have spanned many seasons, including its disappearance from Titan's northern spring stratosphere, with its reemergence in Titan's southern fall stratosphere (Jennings et al. 2012a,b, 2015). No matter the latitude or season, the Haystack's spectral dependence remains the same. This lack of spectral variation, combined with no known corresponding vapor in the stratosphere, implies that the Haystack—similarly to C_4N_2 ice clouds—has a different formation mechanism from that of vapor condensation. Continued experimental efforts are needed to identify the chemical composition of Titan's Haystack.

3.2.4 The HASP Ice Cloud

The *High-Altitude South Polar (HASP) cloud* is a name given to the CIRS-discovered massive cloud system that developed at altitudes throughout Titan's mid stratosphere at high southern polar latitudes during late southern fall in 2015 (Anderson et al. 2017, 2018, see Figs. 1, 8, 10, 15). The CIRS HASP cloud was first observed in the far-IR near Titan's south pole in March 2015 and the last observation occurred in February 2016, when Cassini began to ramp back up into a higher inclined orbital configuration, preventing further close-in far-IR limb observations of Titan's south polar stratosphere. Between March 2015 and February 2016, the CIRS HASP cloud was always observed at high southern polar latitudes, but at distinctly lower altitudes than the ISS-discovered south polar cloud, which was observed near 300 km.

Figures 15 and 17 show far-IR limb integrations in late southern fall (2015) at 79°S (upper spectra in Figs. 15 and 17) compared to those recorded 10 years earlier in Titan's mid northern winter (2005) at 85°N (lower spectra in Figs. 15 and 17), with the CIRS FP1 FOVs centered on ~ 125 km in Fig. 15 and ~ 225 km in Fig. 17. Noticeable immediately in Fig. 15 is the appearance of a spectral mismatch between the Haystack at 79°S compared to the Haystack at 85°N . The spectral dependence of the Haystack is actually unaltered—the broad shoulder appearing to the lefthand side of the Haystack at 79°S is due to the CIRS HASP cloud. Likewise, in Fig. 17, in which the FP1 FOV is centered at a tangent height 100 km higher in the stratosphere than in Fig. 15, trace amounts of the Haystack material in Titan's stratosphere are observed in these limb integration spectra, both at 85°N and at 79°S , whereas the strong spectral signature from the CIRS HASP cloud is only evident at 79°S . All of the apparent spectral pollutions result from CIRS operating in the limb integration mode. In this scenario, the large CIRS FP1 FOV collects the signal from many altitudes simultaneously during a limb integration, picking up on the HASP cloud opacity from 100 km

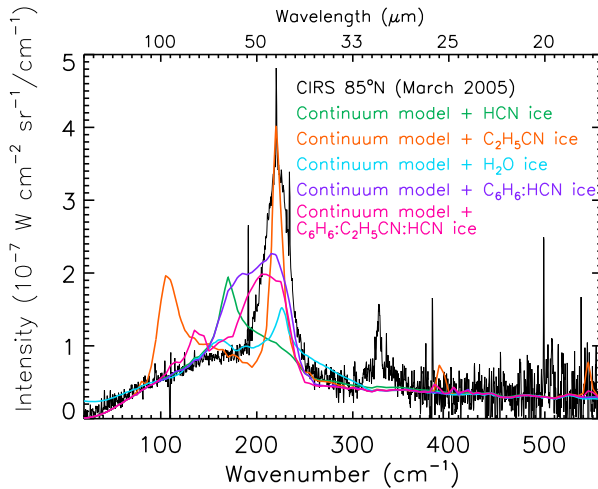


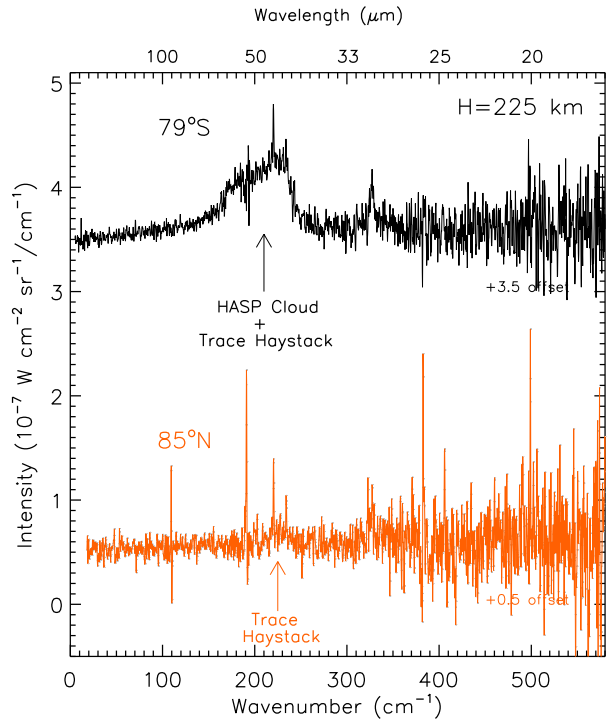
Fig. 16 CIRS far-IR limb integration spectrum at 85°N recorded during mid northern winter in March 2005 (black curve), showing the spectral dependence and intensity contribution to Titan’s stratosphere from the Haystack. The various color-coded curves are synthetic spectra generated from our continuum model at 85°N (Anderson and Samuelson 2011; Anderson et al. 2014, 2018) for five different ices (Mie scattering calculations were performed with a 2 μm particle radius): water ice (aqua curve; vapor was deposited at 140 K; from Hudson and Moore 1995), pure $\text{C}_2\text{H}_5\text{CN}$ ice (orange curve; vapor was deposited at 135 K; from Nna-Mvondo et al. 2018), pure HCN ice (green curve; vapor was deposited at 110 K; from Anderson et al. 2018), co-condensed C_6H_6 :HCN ice in a 4:1 mixing ratio (purple curve; mixed vapors were deposited at 110 K; from Anderson et al. 2017), and co-condensed C_6H_6 : $\text{C}_2\text{H}_5\text{CN}$:HCN ice in a 3.8:1.4:1.0 mixing ratio (pink curve; mixed vapors were deposited at 110 K; from Nna-Mvondo et al. 2018). One of the main reasons that pure $\text{C}_2\text{H}_5\text{CN}$ ice was ruled out as a Haystack candidate was due to its strong low-energy lattice mode, easily seen in the figure (orange curve), and never observed by CIRS (Samuelson et al. 2007). However, during co-condensation formation processes, the $\text{C}_2\text{H}_5\text{CN}$ lattice mode is easily damped out, as is the HCN libration mode

higher up in the stratosphere when the FOV is centered on 125 km and also picking up on the Haystack’s opacity 100 km deeper down in the stratosphere when the FOV is centered on 225 km. As radiative transfer analyses of far-IR limb scans show the CIRS HASP cloud and the Haystack are vertically separated by ~ 100 km (seen also in Fig. 8)—the CIRS HASP cloud vertically resides near 210 km and the Haystack is located near 110 km in July 2015. CIRS data analyses of the low spectral resolution far-IR limb scans must be utilized to unambiguously retrieve the vertical distributions and spectral dependences for all of Titan’s stratospheric particulates.

The spectral dependence of the CIRS HASP cloud is directly connected to its chemical composition (as is true for all other stratospheric particulates). The CIRS-derived spectral dependence of the HASP cloud is shown in Fig. 18, while Fig. 19 depicts the spectral dependences between the HASP cloud and the 160 cm^{-1} ice cloud. The disparate spectral dependences amongst the two clouds—observed 10 years apart—demonstrates that the two ice clouds are comprised of different chemical compositions.

The vertical extent of the CIRS HASP cloud is observed at stratospheric altitudes where the pure compounds HCN, HC_3N , and C_6H_6 are all expected to condense and form stratospheric ice clouds (Fig. 1). As with the northern winter 160 cm^{-1} ice cloud, whose formation mechanism is consistent with simultaneous saturation of HCN and HC_3N , *i.e.*, co-condensation, a similar formation scenario is expected for the CIRS HASP cloud, poten-

Fig. 17 CIRS far-IR limb integrations recorded at 79°S in late southern fall (black curve; July 2015) and at 85°N in mid northern winter (orange curve; March 2005), with the FPI FOV centered on ~225 km. Noticeable immediately is a spectral difference between the two latitudes, with only trace amounts of Haystack material contributing to these limb integration spectra. The strong spectral signature observed at 79°S is due to the HASP cloud, which resides ~100 km higher in the stratosphere than the Haystack. The observed spectral pollutions result from the large range in stratospheric altitudes averaged over the FPI FOV during the limb integrations



tially comprised of co-condensed ice particles containing combinations of HCN, HC₃N, and C₆H₆. Thin ice film transmission spectroscopy targeting ice mixtures containing variable amounts of HCN, HC₃N, and C₆H₆ have been reported by Anderson et al. (2017), with their results indicating that the CIRS HASP cloud's chemical composition is consistent with a co-condensed C₆H₆:HCN ice containing ~80% C₆H₆ and ~20% HCN; this is shown in Fig. 18.

3.2.5 Other Potential Ice Clouds

More efforts have been put forth to describe additional opacity signatures from presumed stratospheric ice clouds. One example was found at 58°S during northern winter, and in addition to the 160 cm⁻¹ ice cloud that was observed near ~90 km, an additional ice cloud was found about 30 km deeper in the stratosphere, peaking at 60 km (Anderson and Samuelson 2011). The altitude location combined with the far-IR spectral dependence peaking near 80 cm⁻¹ indicated that this ice cloud was composed of condensed C₂H₆ ice. However, far-IR targeted thin ice film transmission spectroscopy experiments are still needed to confirm this chemical identity.

The second example involves the ν_6 band of pure C₆H₆ ice at 682 cm⁻¹. This ice spectral feature was reported to explain some of the stratospheric ice emission features observed in CIRS mid-IR nadir (in May 2013) and limb (in March 2015) spectra (Vinatier et al. 2018). Most notably for the limb spectra spanning 168 km to 278 km, the observed width of the observed ice emission features were reported to be significantly broader than those shown for the ν_6 band of pure C₆H₆ ice at 682 cm⁻¹. Even so, an upper limit of 1.5 μ m for the C₆H₆ particle radius was reported. Three additional spectral peaks at ~687, 695, and ~702 cm⁻¹

Fig. 18 Black curve represents the CIRS-derived spectral dependence of Titan's HASP cloud discovered at mid stratospheric altitudes during late southern fall at 79°S (July 2015). The magenta curve depicts a co-condensed thin ice film (vapors deposited at 110 K) containing ~20% HCN and ~80% C₆H₆. This result demonstrates that the HASP cloud's chemical identification is consistent with a mixed C₆H₆:HCN ice, formed via co-condensation processes

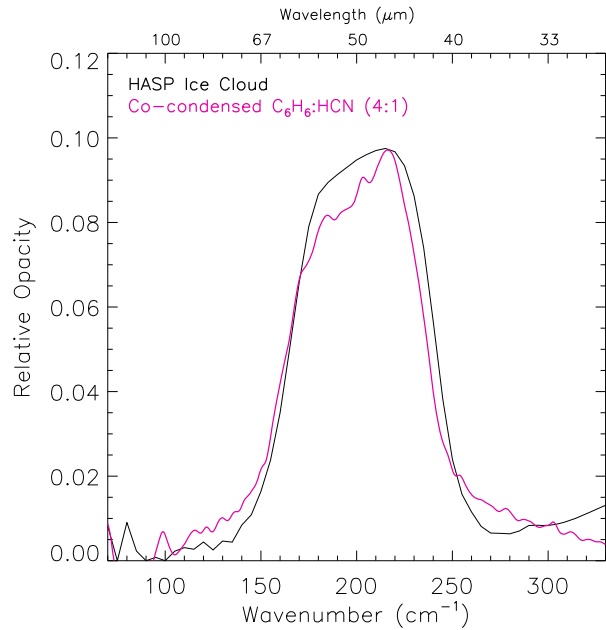
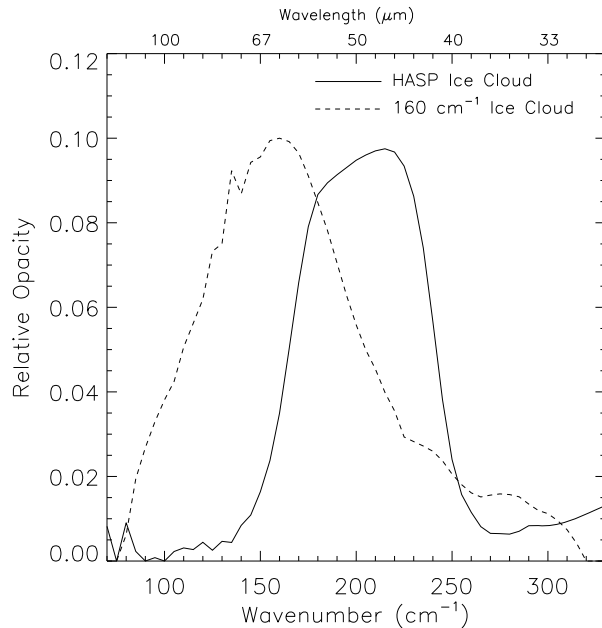


Fig. 19 CIRS-derived spectral dependences of Titan's late southern fall HASP cloud (black solid curve) and the northern winter 160 cm⁻¹ ice cloud (black dashed curve). The dissimilar spectral dependences demonstrate that the two ice clouds—observed 10 years apart in opposite hemispheres—are comprised of different chemical compositions



were also reported, although the investigators could not reproduce these spectral features with the refractive indices found in the literature from the pure nitrile ices HCN, HC₃N, CH₃CN (acetonitrile), C₂H₅CN, or C₂N₂. The four observed spectral signatures may indeed result from co-condensed ices, although dedicated thin ice film transmission spectroscopy

for mixtures containing C_6H_6 are still needed—at various deposition temperatures—to spectrally match the opacity spectral signatures reported by Vinatier et al. (2018).

4 Titan Stratospheric Ice Experimental Efforts

The first experimental laboratory study to interpret ice emission features observed in Titan's north polar stratosphere by IRIS was performed in the far-IR by Khanna et al. (1987). The investigators identified the IRIS-observed ice emission feature at 478 cm^{-1} as the ν_8 band of crystalline C_4N_2 ice. The C_4N_2 vapor was deposited at 70 K, warmed to 90 K, and then annealed. Experimental studies continued in the mid-IR with C_2H_2 and C_4H_2 ice (Khanna et al. 1988). Even though these hydrocarbon ices were not observed by IRIS, Khanna et al. (1988) claimed that they may reside in Titan's lower stratosphere given their very strong observed vapor emission features in the mid-IR. Subsequent experiments in the mid-IR were performed involving HCN, HC_3N , and C_4N_2 (Masterson and Khanna 1990). HCN vapor was deposited at 60 K, then the ice was warmed and annealed at 80 K for 30 minutes. Both HC_3N and C_4N_2 vapors were deposited at 70 K, then warmed and annealed at 90 K for 30 minutes. The fundamental vibrational modes and combination or overtone bands of the ice spectral peaks detected were assigned across the wavenumber range $450\text{--}5000\text{ cm}^{-1}$, and also their complex refractive indices were calculated.

Next, an extensive laboratory effort was initiated involving HCN, HC_3N , CH_3CN , C_2H_5CN , C_2H_3CN , C_2N_2 , and C_4N_2 , spanning wavenumbers 80 to 5000 cm^{-1} (Dello Russo and Khanna 1996). The vapors were deposited somewhere between 50 and 100 K, and annealed at various temperatures (see Table 1), then cooled to 95 K and 35 K, where their transmittance spectra were recorded. This was the first detailed laboratory effort demonstrating the strong low-energy vibrational modes of Titan-relevant nitrile ices in the far-IR, especially below 200 cm^{-1} . Following this experimental effort, a focused study on C_2H_5CN ice was put forth, in an effort to chemically identify Titan's Haystack (Khanna 2005). Whereas earlier work regarding C_2H_5CN ice performed by Dello Russo and Khanna (1996) showed C_2H_5CN ice had a strong spectral feature at 225 and 226 cm^{-1} (due to the ν_{13} C–C \equiv N bending mode), the re-examination of C_2H_5CN ice by Khanna (2005) revealed that the ν_{13} band had shifted to 221 cm^{-1} . The 4 to 5 cm^{-1} wavenumber shift resulted from annealing C_2H_5CN ice at 120 K (compared to 140 K from the earlier experiment) and also the annealing time duration was much longer (4 to 5 hours). Additional discrepancies at higher energies were also found. More recently, a very detailed study of C_2H_5CN ice, with a focus on better understanding Titan's CIRS-observed stratospheric ice clouds, especially in regards to the Haystack, was reported for vapor deposition temperatures ranging from 30 K to 150 K (Nna-Mvondo et al. 2018).

In the Cassini era, the first Titan-relevant experimental study was performed by Moore et al. (2010). Both the amorphous and crystalline phases of HCN, HC_3N , CH_3CN , C_2H_5CN , and C_2N_2 , spanning wavenumbers 30 to 5000 cm^{-1} were measured, as well as determinations of their complex refractive indices. As with all the previous Titan-related thin ice film transmission spectroscopy studies, all the vapors were deposited at cold temperatures (*e.g.*, 30 K), ensuring the amorphous phase was achieved, and then annealed to warmer temperatures for their transition to the crystalline phase (see Tables 1 and 2 for details, as well as Anderson et al. 2018).

In order to interpret and chemically identify many of the CIRS-discovered stratospheric ice clouds, a new experimental approach, modified from all the previous Titan ice work, was needed. As discussed in Sects. 1 and 3, Titan's stratospheric ice clouds commonly form as

Table 1 Summary of crystalline phase laboratory studies related to Titan's stratospheric ice clouds

Compound	Experimental conditions	Spectral range	Published work
HCN	deposited at 60 K annealed for 30 min at 80 K	450–5000 cm ⁻¹	Masterson and Khanna (1990)
	deposited between 50 and 100 K annealed for 30 to 180 min at 120 K cooled to 95 K, 35 K	80–5000 cm ⁻¹	Dello Russo and Khanna (1996)
	deposited at 50 K annealed at 120 K for 120 min in mid-IR annealed at 120 K for 80 min in far-IR cooled to 20 K, 35 K, 50 K, 75 K, 95 K, 110 K	30–5000 cm ⁻¹	Moore et al. (2010)
HC ₃ N	deposited at 70 K annealed 30 min at 90 K cooled to 60 K	450–4000 cm ⁻¹	Masterson and Khanna (1990)
	deposited between 50 and 100 K annealed 30 to 180 min at 110 K cooled to 95 K, 35 K	80–5000 cm ⁻¹	Dello Russo and Khanna (1996)
	deposited at 50 K annealed at 110 K for 120 min in mid-IR annealed at 110 K for 65 min in far-IR cooled to 20 K, 35 K, 50 K, 75 K, 95 K, 110 K	30–5000 cm ⁻¹	Moore et al. (2010)
C ₂ N ₂	deposited between 50 and 100 K annealed 30 to 180 min at 90 K cooled to 95 K, 35 K	80–5000 cm ⁻¹	Dello Russo and Khanna (1996)
	deposited at 20 K annealed at 90 K for 60 min in mid-IR annealed at 90 K for 90 min in far-IR cooled to 20 K, 35 K, 50 K, 75 K	30–5000 cm ⁻¹	Moore et al. (2010)
C ₄ N ₂	deposited at 70 K annealed 30 min at 90 K also annealed at 155 K	400–4000 cm ⁻¹	Khanna et al. (1987)
	deposited at 70 K annealed 30 min at 90 K cooled to 60 K	450–4000 cm ⁻¹	Masterson and Khanna (1990)
	deposited between 50 and 100 K annealed 30 to 180 min at 120 K cooled to 95 K, 35 K	80–5000 cm ⁻¹	Dello Russo and Khanna (1996)
CH ₃ CN	deposited between 50 and 100 K annealed 30 to 180 min at 130 K cooled to 95 K, 35 K	80–5000 cm ⁻¹	Dello Russo and Khanna (1996)
	deposited at 50 K annealed 66 min at 130 K in mid-IR annealed 45 min at 130 K in far-IR cooled to 20 K, 35 K, 50 K, 75 K, 95 K, 110 K	30–5000 cm ⁻¹	Moore et al. (2010)
	collisional cooling cell particles formed at 95 K, 110 K, 130 K	50–5000 cm ⁻¹	Ennis et al. (2017)
C ₂ H ₃ CN	deposited between 50 and 100 K annealed 30 to 180 min at 130 K cooled to 95 K, 35 K	80–5000 cm ⁻¹	Dello Russo and Khanna (1996)

Table 1 (Continued)

Compound	Experimental conditions	Spectral range	Published work
C ₂ H ₅ CN	deposited between 50 and 100 K annealed 30 to 180 min at 140 K cooled to 95 K, 35 K	80–5000 cm ⁻¹	Dello Russo and Khanna (1996)
	deposited at 60 K annealed 4 to 5 hours at 120 K	200–7800 cm ⁻¹	Khanna (2005)
	deposited at 50 K annealed at 140 K for 90 min in mid-IR annealed at 140 K for 92 min in far-IR cooled to 20 K, 35 K, 50 K, 75 K, 95 K, 110 K	30–5000 cm ⁻¹	Moore et al. (2010)
	collisional cooling cell particles formed at 95 K, 110 K, 130 K	50–5000 cm ⁻¹	Ennis et al. (2017)
C ₃ H ₃ CN	deposited between 50 and 100 K annealed 30 to 180 min at 145 K cooled to 95 K, 35 K	80–5000 cm ⁻¹	Dello Russo and Khanna (1996)

Table 2 Summary of Amorphous phase laboratory studies related to Titan's stratospheric ice clouds

Compound	Experimental conditions	Spectral range	Published work
HCN	deposited at 50 K warmed to 75 K, 95 K, 110 K	30–5000 cm ⁻¹	Moore et al. (2010)
HC ₃ N	deposited at 50 K warmed to 50 K, 75 K, 95 K	30–5000 cm ⁻¹	Moore et al. (2010)
C ₂ N ₂	deposited at 20 K warmed to 35 K, 50 K, 75 K	30–5000 cm ⁻¹	Moore et al. (2010)
CH ₃ CN	deposited at 50 K warmed to 75 K, 95 K, 110 K	30–5000 cm ⁻¹	Moore et al. (2010)
C ₂ H ₅ CN	deposited at 50 K warmed to 75 K, 95 K, 110 K	30–5000 cm ⁻¹	Moore et al. (2010)

a result of the vapors diffusing/subsiding, cooling as they descend in Titan's stratosphere, then condensing once saturation has been achieved. Many of these vapors will enter altitude regions where they will undergo simultaneous saturation, thus forming co-condensed ice clouds. Thin ice film transmission spectroscopy for the purpose of studying Titan's stratospheric ice clouds must therefore be performed with vapor deposition at temperatures > 100 K. This is necessary since the structure of the ice, for both pure and mixtures, is modified between annealing and warm-deposition experiments (this is expanded on in Anderson et al. 2018). The main reason is that during annealing experiments, a complete ordering of the ice structure is not achieved, so a portion of the amorphous structure is irretrievably retained in the final crystalline phase. These differences are more pronounced in the low-energy part of the far-IR. Using C₂H₅CN ice as an example, Khanna (2005) reported that the longer time required for annealing C₂H₅CN ice, compared to other nitriles, is necessary since there may be several possible orientations of the methyl (CH₃) and methylene groups (CH₂) in the solid phase when the samples are quenched at low temperatures, thus causing low barriers in the rotation of these groups around the single bonds. These effects

are most noticeable in the low energy lattice modes, as recently detailed in a comprehensive laboratory study on the ice phases of C_2H_5CN (Nna-Mvondo et al. 2018).

C_2H_5CN ice was also recently studied by Ennis et al. (2017), in which C_2H_5CN and CH_3CN ice particles were generated at 95 K, 110 K, and 130 K under simulated Titan temperature and pressure conditions using collisional cooling cell experiments. The investigators measured transmittance spectra from 50 to 5000 cm^{-1} , with a focus in the far-IR to study the morphology of the icy particulates, identify their crystalline phases, and also attempt to spectrally match the Haystack. While a metastable b-phase (monoclinic) ice was identified for CH_3CN , there was no such phase observed for C_2H_5CN . Ennis et al. (2017) also reported the $200\text{--}250\text{ cm}^{-1}$ region was absent of an CH_3CN spectral feature, but found the ν_{13} band of crystalline C_2H_5CN ice at 110 K was located at 226 cm^{-1} , which is in agreement with Dello Russo and Khanna (1996).

Reproducing Titan's stratospheric ices in the laboratory requires forming the ice samples with both high purity and free of oxygen-bearing components. Whereas some of the nitriles and hydrocarbons necessary for Titan ice experiments are available commercially by chemical manufacturers (e.g., C_2H_5CN , CH_3CN , C_2H_2), others like HCN , HC_3N , C_2N_2 , C_4N_2 , and C_4H_2 must be synthesized in the laboratory. No matter the way in which the compounds are secured, all will likely contain some degree of contamination, such as the air contaminants H_2O and CO_2 , byproducts from the syntheses, or additional organics produced from exposing nitriles to ambient air. The presence of any sample impurity must be purged since it can alter the spectral features of the Titan ice analogs, ultimately resulting in inaccurately-determined complex refractive indices. Purifying the sample becomes very crucial, and unfortunately, most of the published laboratory work focused on Titan's stratospheric ices are impure. For example, some work efforts report CO_2 impurity bands in the infrared spectra of their synthesized ices, e.g., in the HC_3N spectra reported in Moore et al. (2010), in the C_4N_2 ice spectrum of Khanna et al. (1987), and in the CH_3CN ice spectrum of Ennis et al. (2017). This latter work effort also noted the cryopump oil impurities in their samples. They further showed the presence of CO_2 as an impurity in their CH_3CN and C_2H_5CN ice particle spectra (both generated from the purified commercial nitriles). CO_2 was introduced as an impurity in the dry N_2 bath gas as well as an adsorbed formic acid remnant from previous experiments. Moreover, their C_2H_5CN ice particle spectra also contained traces of acetonitrile absorbed on the enclosed flow cooling cell or on the deposition line walls. Additionally, when purchased chemicals are used, and no purification is performed, the resulting absorbance spectra can contain air contaminants such as CO_2 , e.g., in the C_2N_2 ice spectra of Moore et al. (2010), or H_2O , e.g., in the C_2H_5CN ice spectra of Khanna (2005). In recent work, however, Anderson et al. (2018) illustrates the difficulties in synthesizing the initial compounds needed for the Titan stratospheric ice experiments, the efforts and time dedication involved in purifying the sample, and the corresponding benefits that are reflected in the recorded transmittance spectra. These investigators also discuss their new Titan ice chamber, focus on simulating Titan's icy stratospheric environment, with an emphasis on the formation of co-condensed ices.

5 Closing Remarks

Many of the extensive laboratory efforts focused on thin ice film transmission spectroscopy over the last three decades (see for example Allamandola et al. 1988; Sandford and Allamandola 1993a,b; Hudgins et al. 1993; Bohn et al. 1994; Bernstein et al. 1997; Allamandola et al. 1999; Moore et al. 2007; Hudson et al. 2009, 2014; Bouwman et al. 2010; Gerakines and

Hudson 2015) have been astrochemistry-driven and/or aimed at the interpretation of ground- and/or space-based observations of interstellar ices, ices in molecular clouds, as well as ices on airless bodies (or with tenuous atmospheres) in the solar system, *e.g.*, comets, Triton, Pluto, asteroids, etc. Except for the experiments listed in Sect. 4, very few have focused on simulating and reproducing Titan's stratospheric ice clouds, especially those observed by Cassini's ISS, VIMS, or CIRS instruments. This is a direct result of limited observational data, with most laboratory efforts regarding Titan's stratospheric ices, aimed at interpreting Voyager 1 IRIS-derived results obtained during the Titan north polar limb mosaic recorded in 1980. It was not until Cassini arrived in the Saturn system in 2004, combined with its 13-year mission tenure, that observations of ice clouds residing in Titan's stratosphere over multiple seasons were acquired, resulting in the need for much more detailed experimental studies. Specifically, these experiments must be performed by depositing the vapor at temperatures that are representative of Titan's stratosphere, ideally at temperatures between ~ 67 K and 150 K. Dedicated thin ice film transmission spectroscopy experimental efforts are critically needed to better understand the chemical compositions, optical properties, and formation mechanisms of Titan's observed stratospheric ice clouds. This is especially true regarding co-condensed ices and for ices that do not form from vapor condensation processes, *i.e.*, C_4N_2 ice, the Haystack, etc.

Titan's stratospheric ice cloud structures are very complex, and these clouds play an especially important radiative role where they spatially exist in Titan's stratosphere. They are significant sources of thermal infrared opacity, especially at winter polar latitudes, contributing significantly to Titan's atmospheric radiative balance. For example, based on the sheer strength in intensity of the Haystack (it is ~ 50 times more opaque than the aerosol at 221 cm^{-1} during northern winter at 85°N), it appears to provide an exceptionally strong radiative cooling mechanism where it resides spatially, with additional contribution from the other stratospheric ice clouds. Both the Haystack and Titan's additional stratospheric clouds are all very efficient far-IR radiative coolers, which leads to significant and unexpected alterations to Titan's vertical temperature structures, especially in the winter polar stratosphere (Schinder et al. 2011, 2012; Anderson et al. 2014). The vertical extent of the Haystack appears to correspond very closely to the location of Titan's local stratospheric temperature minimum near 110 km at 85°N during northern winter (Anderson et al. 2014). Other local stratospheric temperature minima occur as well in the late southern fall season. Continued radiative transfer analyses, radiative cooling calculations, along with ongoing experimental efforts, are critically needed to better understand the contributions from all of Titan's stratospheric ice clouds.

Acknowledgements C.M. Anderson and R.E. Samuelson acknowledge funding from both the Cassini Project and the Cassini Data Analysis Program. D. Nna-Mvondo acknowledges funding from the NASA Postdoctoral Program at GSFC, administered by the University Space Research Association through a contract with NASA.

Open Access This article is distributed under the terms of the Creative Commons Attribution 4.0 International License (<http://creativecommons.org/licenses/by/4.0/>), which permits unrestricted use, distribution, and reproduction in any medium, provided you give appropriate credit to the original author(s) and the source, provide a link to the Creative Commons license, and indicate if changes were made.

References

- R.K. Achterberg, B.J. Conrath, P.J. Gierasch, F.M. Flasar, C.A. Nixon, Titan's middle-atmospheric temperatures and dynamics observed by the Cassini Composite Infrared Spectrometer. *Icarus* **194**, 263–277 (2008)

- R.K. Achterberg, P.J. Gierasch, B.J. Conrath, F.M. Flasar, C.A. Nixon, Temporal variations of Titan's middle-atmospheric temperatures from 2004 to 2009 observed by Cassini/CIRS. *Icarus* **211**, 686–698 (2011)
- L.J. Allamandola, S.A. Sandford, G.J. Valero, Photochemical and thermal evolution of interstellar/precometary ice analogs. *Icarus* **76**, 225–252 (1988)
- L.J. Allamandola, M.P. Bernstein, S.A. Sandford, R.L. Walker, Evolution of interstellar ices. *Space Sci. Rev.* **90**, 219–232 (1999)
- C.M. Anderson, R.E. Samuelson, Titan's aerosol and stratospheric ice opacities between 18 and 500 μm : vertical and spectral characteristics from Cassini CIRS. *Icarus* **212**, 762–778 (2011)
- C.M. Anderson, R.E. Samuelson, G.L. Bjoraker, R.K. Achterberg, Particle size and abundance of HC_3N ice in Titan's lower stratosphere at high northern latitudes. *Icarus* **207**, 914–922 (2010)
- C.M. Anderson, R.E. Samuelson, R.K. Achterberg, J.W. Barnes, F.M. Flasar, Subsidence-induced methane clouds in Titan's winter polar stratosphere and upper troposphere. *Icarus* **243**, 129–138 (2014)
- C.M. Anderson, R.E. Samuelson, Y.L. Yung, J.L. McLain, Solid-state photochemistry as a formation mechanism for Titan's stratospheric C_4N_2 ice clouds. *Geophys. Res. Lett.* **43**, 3088–3094 (2016)
- C. Anderson, D. Nna-Mvondo, R.E. Samuelson, R.K. Achterberg, F.M. Flasar, D.E. Jennings, F. Raulin, Titan's High Altitude South Polar (HASP) stratospheric ice cloud as observed by Cassini CIRS, in *AAS/Division for Planetary Sciences Meeting Abstracts*, vol. 49 (2017), 304.10
- C.M. Anderson, D. Nna-Mvondo, R.E. Samuelson, J.L. McLain, J.P. Dworkin, The SPECTRAL ice chamber: application to Titan's stratospheric ice clouds. *Astrophys. J.* **865**, 62 (2018), 12 pp.
- E.L. Barth, Modeling survey of ices in Titan's stratosphere. *Planet. Space Sci.* **137**, 20–31 (2017)
- M.P. Bernstein, L.J. Allamandola, S.A. Sandford, Complex organics in laboratory simulations of interstellar/cometary ices. *Adv. Space Res.* **19**, 991–998 (1997)
- R.B. Bohn, S.A. Sandford, L.J. Allamandola, D.P. Cruikshank, Infrared spectroscopy of Triton and Pluto ice analogs: the case for saturated hydrocarbons. *Icarus* **111**, 151–173 (1994)
- J. Bouwman, H.M. Cuppen, A. Bakker, L.J. Allamandola, H. Linnartz, Photochemistry of the PAH pyrene in water ice: the case for ion-mediated solid-state astrochemistry. *Astron. Astrophys.* **511**, A33 (2010). [arXiv:0911.1750](https://arxiv.org/abs/0911.1750)
- A.J. Coates, A. Wellbrock, G.R. Lewis, G.H. Jones, D.T. Young, F.J. Cray, J.H. Waite, Heavy negative ions in Titan's ionosphere: altitude and latitude dependence. *Planet. Space Sci.* **57**, 1866–1871 (2009)
- A. Coustenis, B. Bezard, Titan's atmosphere from Voyager infrared observations. 4: Latitudinal variations of temperature and composition. *Icarus* **115**, 126–140 (1995)
- A. Coustenis, B. Schmitt, R.K. Khanna, F. Trotta, Plausible condensates in Titan's stratosphere from Voyager infrared spectra. *Planet. Space Sci.* **47**, 1305–1329 (1999)
- A. Coustenis, R.K. Achterberg, B.J. Conrath, D.E. Jennings, A. Marten, D. Gautier, C.A. Nixon, F.M. Flasar, N.A. Teanby, B. Bézard, R.E. Samuelson, R.C. Carlson, E. Lellouch, G.L. Bjoraker, P.N. Romani, F.W. Taylor, P.G. Irwin, T. Fouchet, A. Hubert, G.S. Orton, V.G. Kunde, S. Vinatier, J. Mondellini, M.M. Abbas, R. Courtin, The composition of Titan's stratosphere from Cassini/CIRS mid-infrared spectra. *Icarus* **189**, 35–62 (2007)
- A. Coustenis, D.E. Jennings, R.K. Achterberg, G. Bampasidis, P. Lavvas, C.A. Nixon, N.A. Teanby, C.M. Anderson, V. Cottini, F.M. Flasar, Titan's temporal evolution in stratospheric trace gases near the poles. *Icarus* **270**, 409–420 (2016)
- A. Coustenis, D.E. Jennings, R.K. Achterberg, G. Bampasidis, C.A. Nixon, P. Lavvas, V. Cottini, F.M. Flasar, Seasonal evolution of Titan's stratosphere near the poles. *Astrophys. J.* **854**, L30 (2018)
- R. de Kok, P.G.J. Irwin, N.A. Teanby, C.A. Nixon, D.E. Jennings, L. Fletcher, C. Howett, S.B. Calcutt, N.E. Bowles, F.M. Flasar, F.W. Taylor, Characteristics of Titan's stratospheric aerosols and condensate clouds from Cassini CIRS far-infrared spectra. *Icarus* **191**, 223–235 (2007)
- R. de Kok, P.G.J. Irwin, N.A. Teanby, Condensation in Titan's stratosphere during polar winter. *Icarus* **197**, 572–578 (2008)
- R.J. de Kok, N.A. Teanby, L. Maltagliati, P.G.J. Irwin, S. Vinatier, HCN ice in Titan's high-altitude southern polar cloud. *Nature* **514**, 65–67 (2014). [arXiv:1410.5563](https://arxiv.org/abs/1410.5563)
- N. Dello Russo, R.K. Khanna, Laboratory infrared spectroscopic studies of crystalline nitriles with relevance to outer planetary systems. *Icarus* **123**, 366–395 (1996)
- L.R. Doose, E. Karkoschka, M.G. Tomasko, C.M. Anderson, Vertical structure and optical properties of Titan's aerosols from radiance measurements made inside and outside the atmosphere. *Icarus* **270**, 355–375 (2016)
- C. Ennis, R. Auchtell, M. Ruzi, E.G. Robertson, Infrared characterisation of acetonitrile and propionitrile aerosols under Titan's atmospheric conditions. *Phys. Chem. Chem. Phys.* **19**, 2915–2925 (2017). Incorporating Faraday transactions
- E.F. Erickson, R.F. Knacke, A.T. Tokunaga, M.R. Haas, The 45 micron H_2O ice band in the Kleinmann–Low nebula. *Astrophys. J.* **245**, 148–153 (1981)

- F.M. Flasar, R.K. Achterberg, The structure and dynamics of Titan's middle atmosphere. *Philos. Trans. R. Soc. A* **367**, 649–664 (2009). <https://doi.org/10.1098/rsta.2008.0242>
- F.M. Flasar, R.E. Samuelson, B.J. Conrath, Titan's atmosphere: temperature and dynamics. *Nature* **292**, 693–698 (1981)
- F.M. Flasar, R.K. Achterberg, B.J. Conrath, P.J. Gierasch, V.G. Kunde, C.A. Nixon, G.L. Bjoraker, D.E. Jennings, P.N. Romani, A.A. Simon-Miller, B. Bézard, A. Coustenis, P.G.J. Irwin, N.A. Teanby, J. Brasunas, J.C. Pearl, M.E. Segura, R.C. Carlson, A. Mamoutkine, P.J. Schinder, A. Barucci, R. Courtin, T. Fouchet, D. Gautier, E. Lellouch, A. Marten, R. Prange, S. Vinatier, D.F. Strobel, S.B. Calcutt, P.L. Read, F.W. Taylor, N. Bowles, R.E. Samuelson, G.S. Orton, L.J. Spilker, T.C. Owen, J.R. Spencer, M.R. Showalter, C. Ferrari, M.M. Abbas, F. Raulin, S. Edgington, P. Ade, E.H. Wishnow, Titan's atmospheric temperatures, winds, and composition. *Science* **308**, 975–978 (2005)
- N. Fray, B. Schmitt, Sublimation of ices of astrophysical interest: a bibliographic review. *Planet. Space Sci.* **57**, 2053–2080 (2009)
- C. Frère, F. Raulin, G. Israel, M. Cabane, Microphysical modeling of Titan's aerosols—application to the in situ analysis. *Adv. Space Res.* **10**, 159–163 (1990)
- P.A. Gerakines, R.L. Hudson, First infrared band strengths for amorphous CO₂, an overlooked component of interstellar ices. *Astrophys. J. Lett.* **808**, L40 (2015)
- C.A. Griffith, P. Penteado, P. Rannou, R. Brown, V. Boudon, K.H. Baines, R. Clark, P. Drossart, B. Buratti, P. Nicholson, C.P. McKay, A. Coustenis, A. Negro, R. Jaumann, Evidence for a polar ethane cloud on Titan. *Science* **313**, 1620–1622 (2006)
- R. Hanel, B. Conrath, F.M. Flasar, V. Kunde, W. Maguire, J.C. Pearl, J. Pirraglia, R. Samuelson, L. Herath, M. Allison, D.P. Cruikshank, D. Gautier, P.J. Gierasch, L. Horn, R. Koppány, C. Ponnampuruma, Infrared observations of the Saturnian system from Voyager 1. *Science* **212**, 192–200 (1981)
- R.A. Hanel, B.J. Conrath, D.E. Jennings, R.E. Samuelson, Retrieval of physical parameters from measurements, in *Exploration of the Solar System by Infrared Remote Sensing* (Cambridge University Press, Cambridge, 2003), pp. 352–404. Chap. 8
- A.G. Hayes, The lakes and seas of Titan. *Annu. Rev. Earth Planet. Sci.* **44**, 57–83 (2016)
- A. Hayes, O. Aharonson, P. Callahan, C. Elachi, Y. Gim, R. Kirk, K. Lewis, R. Lopes, R. Lorenz, J. Lunine, K. Mitchell, G. Mitri, E. Stofan, S. Wall, Hydrocarbon lakes on Titan: distribution and interaction with a porous regolith. *Geophys. Res. Lett.* **35**, L09204 (2008)
- A.G. Hayes, O. Aharonson, J.I. Lunine, R.L. Kirk, H.A. Zebker, L.C. Wye, R.D. Lorenz, E.P. Turtle, P. Pailou, G. Mitri, S.D. Wall, E.R. Stofan, K.L. Mitchell, C. Elachi (Cassini Radar Team), Transient surface liquid in Titan's polar regions from Cassini. *Icarus* **211**, 655–671 (2011)
- S.M. Hörst, Titan's atmosphere and climate. *J. Geophys. Res., Planets* **122**, 432–482 (2017)
- F. Hourdin, S. Lebonnois, D. Luz, P. Rannou, Titan's stratospheric composition driven by condensation and dynamics. *J. Geophys. Res., Planets* **109**(E18), E12005 (2004)
- D.M. Hudgins, S.A. Sandford, L.J. Allamandola, A.G.G.M. Tielens, Mid- and far-infrared spectroscopy of ices—optical constants and integrated absorbances. *Astrophys. J. Suppl. Ser.* **86**, 713–870 (1993)
- R.L. Hudson, M.H. Moore, FAR-IR spectral changes accompanying proton irradiation of solids of astrochemical interest. *Radiat. Phys. Chem.* **45**, 779–789 (1995)
- R.L. Hudson, M.H. Moore, L.L. Raines, Ethane ices in the outer Solar System: spectroscopy and chemistry. *Icarus* **203**, 677–680 (2009)
- R.L. Hudson, R.F. Ferrante, M.H. Moore, Infrared spectra and optical constants of astronomical ices: I. Amorphous and crystalline acetylene. *Icarus* **228**, 276–287 (2014)
- D.E. Jennings, C.M. Anderson, R.E. Samuelson, F.M. Flasar, C.A. Nixon, G.L. Bjoraker, P.N. Romani, R.K. Achterberg, V. Cottini, B.E. Hesman, V.G. Kunde, R.C. Carlson, R. de Kok, A. Coustenis, S. Vinatier, G. Bampasidis, N.A. Teanby, S.B. Calcutt, First observation in the South of Titan's far-infrared 220 cm⁻¹ cloud. *Astrophys. J. Lett.* **761**, L15 (2012a)
- D.E. Jennings, C.M. Anderson, R.E. Samuelson, F.M. Flasar, C.A. Nixon, V.G. Kunde, R.K. Achterberg, V. Cottini, R. de Kok, A. Coustenis, S. Vinatier, S.B. Calcutt, Seasonal disappearance of far-infrared haze in Titan's stratosphere. *Astrophys. J. Lett.* **754**, L3 (2012b)
- D.E. Jennings, R.K. Achterberg, V. Cottini, C.M. Anderson, F.M. Flasar, C.A. Nixon, G.L. Bjoraker, V.G. Kunde, R.C. Carlson, E. Guandique, M.S. Kaelberer, J.S. Tingley, S.A. Albright, M.E. Segura, R. de Kok, A. Coustenis, S. Vinatier, G. Bampasidis, N.A. Teanby, S. Calcutt, Evolution of the far-infrared cloud at Titan's South pole. *Astrophys. J. Lett.* **804**, L34 (2015)
- D.E. Jennings, F.M. Flasar, V.G. Kunde, C.A. Nixon, M.E. Segura, P.N. Romani, N. Gorius, S. Albright, J.C. Brasunas, R.C. Carlson, A.A. Mamoutkine, E. Guandique, M.S. Kaelberer, S. Aslam, R.K. Achterberg, G.L. Bjoraker, C.M. Anderson, V. Cottini, J.C. Pearl, M.D. Smith, B.E. Hesman, R.D. Barney, S. Calcutt, T.J. Vellacott, L.J. Spilker, S.G. Edgington, S.M. Brooks, P. Ade, P.J. Schinder, A. Coustenis, R. Courtin, G. Michel, R. Fettig, S. Pílorz, C. Ferrari, Composite infrared spectrometer (CIRS) on Cassini. *Appl. Opt.* **56**(18), 5274–5294 (2017)

- A. Jolly, V. Cottini, A. Fayt, L. Manceron, F. Kwabia-Tchana, Y. Benilan, J.C. Guillemin, C. Nixon, P. Irwin, Gas phase dicyanoacetylene (C_4N_2) on Titan: new experimental and theoretical spectroscopy results applied to Cassini CIRS data. *Icarus* **248**, 340–346 (2015)
- R.K. Khanna, Condensed species in titan's stratosphere: confirmation of crystalline cyanoacetylene (HC_3N) and evidence for crystalline acetylene (C_2H_2) on Titan. *Icarus* **178**, 165–170 (2005)
- R.K. Khanna, M.A. Perera-Jarmer, M.J. Ospina, Vibrational infrared and Raman spectra of dicyanoacetylene. *Spectrochim. Acta, Part A, Mol. Biomol. Spectrosc.* **43**, 421–425 (1987)
- R.K. Khanna, M.J. Ospina, G. Zhao, Infrared band extinctions and complex refractive indices of crystalline C_2H_2 and C_4H_2 . *Icarus* **73**, 527–535 (1988)
- L.M. Lara, E. Lellouch, J.J. López-Moreno, R. Rodrigo, Vertical distribution of Titan's atmospheric neutral constituents. *J. Geophys. Res.* **101**, 23261–23283 (1996)
- S. Le Mouélic, P. Rannou, S. Rodriguez, C. Sotin, C.A. Griffith, L. Le Corre, J.W. Barnes, R.H. Brown, K.H. Baines, B.J. Buratti, R.N. Clark, P.D. Nicholson, G. Tobie, Dissipation of Titan's North polar cloud at northern spring equinox. *Planet. Space Sci.* **60**, 86–92 (2012)
- S. Le Mouélic, S. Rodriguez, R. Robidel, B. Rousseau, B. Seignovert, C. Sotin, J.W. Barnes, R.H. Brown, K.H. Baines, B.J. Buratti, R.N. Clark, P.D. Nicholson, P. Rannou, T. Cornet, Mapping polar atmospheric features on Titan with VIMS: from the dissipation of the northern cloud to the onset of a southern polar vortex. *Icarus* **311**, 371–383 (2018)
- S. Lebonnois, J. Burgalat, P. Rannou, B. Charnay, Titan global climate model: a new 3-dimensional version of the IPSL Titan GCM. *Icarus* **218**, 707–722 (2012)
- C.B. Leovy, J.B. Pollack, A first look at atmospheric dynamics and temperature variations on Titan. *Icarus* **19**, 195–201 (1973)
- J.M. Lora, J.I. Lunine, J.L. Russell, GCM simulations of Titan's middle and lower atmosphere and comparison to observations. *Icarus* **250**, 516–528 (2015). [arXiv:1412.7995](https://arxiv.org/abs/1412.7995)
- W.C. Maguire, R.A. Hanel, D.E. Jennings, V.G. Kunde, R.E. Samuelson, C_3H_8 and C_3H_4 in Titan's atmosphere. *Nature* **292**, 683–686 (1981)
- C.M. Masterson, R.K. Khanna, Absorption intensities and complex refractive indices of crystalline HCN, HC_3N , and C_4N_2 in the infrared region. *Icarus* **83**, 83–92 (1990)
- L.A. Mayo, R.E. Samuelson, Condensate clouds in Titan's north polar stratosphere. *Icarus* **176**, 316–330 (2005)
- M.J. Molina, T.L. Tso, L.T. Molina, F.C.Y. Wang, Antarctic stratospheric chemistry of chlorine nitrate, hydrogen chloride, and ice: release of active chlorine. *Science* **238**, 1253–1257 (1987)
- M.H. Moore, R.F. Ferrante, R.L. Hudson, J.N. Stone, Ammonia water ice laboratory studies relevant to outer Solar System surfaces. *Icarus* **190**, 260–273 (2007)
- M.H. Moore, R.F. Ferrante, W.J. Moore, R. Hudson, Infrared spectra and optical constants of nitrile ices relevant to Titan's atmosphere. *Astrophys. J. Suppl. Ser.* **191**, 96–112 (2010)
- C.E. Newman, M.I. Richardson, Y. Lian, C. Lee, Simulating Titan's methane cycle with the TitanWRF general circulation model. *Icarus* **267**, 106–134 (2016)
- D. Nna-Mvondo, C.A. Anderson, R.E. Samuelson, Detailed infrared study of propionitrile amorphous and crystalline ices relevant to Titan's stratospheric ice clouds. *Icarus* (2018, submitted)
- C.C. Porco, E. Baker, J. Barbara, K. Beurle, A. Brahic, J.A. Burns, S. Charnoz, N. Cooper, D.D. Dawson, A.D. Del Genio, T. Denk, L. Dones, U. Dyudina, M.W. Evans, S. Fussner, B. Giese, K. Grazier, P. Helfenstein, A.P. Ingersoll, R.A. Jacobson, T.V. Johnson, A. McEwen, C.D. Murray, G. Neukum, W.M. Owen, J. Perry, T. Roatsch, J. Spitale, S. Squyres, P. Thomas, M. Tiscareno, E.P. Turtle, A.R. Vasavada, J. Veverka, R. Wagner, R. West, Imaging of Titan from the Cassini spacecraft. *Nature* **434**, 159–168 (2005)
- K. Rages, J.B. Pollack, Titan aerosols—optical properties and vertical distribution. *Icarus* **41**, 119–130 (1980)
- K. Rages, J.B. Pollack, P.H. Smith, Size estimates of Titan's aerosols based on Voyager high-phase-angle images. *J. Geophys. Res.* **88**, 8721–8728 (1983)
- P. Rannou, S. Le Mouélic, C. Sotin, R.H. Brown, Cloud and haze in the winter polar region of Titan observed with Visual and Infrared Mapping Spectrometer on board Cassini. *Astrophys. J.* **748**, 4 (2012)
- F. Raulin, T. Owen, Organic chemistry and exobiology on Titan. *Space Sci. Rev.* **104**, 377–394 (2002)
- S. Rodriguez, S. Le Mouélic, P. Rannou, C. Sotin, R.H. Brown, J.W. Barnes, C.A. Griffith, J. Burgalat, K.H. Baines, B.J. Buratti, R.N. Clark, P.D. Nicholson, Titan's cloud seasonal activity from winter to spring with Cassini/VIMS. *Icarus* **216**, 89–110 (2011)
- H.G. Roe, A.H. Bouchez, C.A. Trujillo, E.L. Schaller, M.E. Brown, Discovery of temperate latitude clouds on Titan. *Astrophys. J. Lett.* **618**, L49–L52 (2005)
- C. Sagan, W.R. Thompson, Production and condensation of organic gases in the atmosphere of Titan. *Icarus* **59**, 133–161 (1984)
- R.E. Samuelson, Clouds and aerosols of Titan's atmosphere, in *The Atmospheres of Saturn and Titan*. Proc. Int. Workshop, vol. ESA SP-241 (1985)

- R.E. Samuelson, Clouds and aerosols of Titan's atmosphere, in *Proceeding Symposium on Titan*, vol. ESA SP-338 (1992)
- R.E. Samuelson, L.A. Mayo, Thermal infrared properties of Titan's stratospheric aerosol. *Icarus* **91**, 207–219 (1991)
- R.E. Samuelson, L.A. Mayo, M.A. Knuckles, R.J. Khanna, C₄N₂ ice in Titan's North polar stratosphere. *Planet. Space Sci.* **45**, 941–948 (1997)
- R.E. Samuelson, M.D. Smith, R.K. Achterberg, J.C. Pearl, Cassini CIRS update on stratospheric ices at Titan's winter pole. *Icarus* **189**, 63–71 (2007)
- S.A. Sandford, L.J. Allamandola, Condensation and vaporization studies of CH₃OH and NH₃ ices: major implications for astrochemistry. *Astrophys. J.* **417**, 815–825 (1993a)
- S.A. Sandford, L.J. Allamandola, The condensation and vaporization behavior of ices containing SO₂, H₂S, and CO₂—implications for Io. *Icarus* **106**, 478 (1993b)
- P.J. Schinder, F.M. Flasar, E.A. Marouf, R.G. French, C.A. McGhee, A.J. Kliore, N.J. Rappaport, E. Barbinis, D. Fleischman, A. Anabtawi, The structure of Titan's atmosphere from Cassini radio occultations. *Icarus* **215**, 460–474 (2011)
- P.J. Schinder, F.M. Flasar, E.A. Marouf, R.G. French, C.A. McGhee, A.J. Kliore, N.J. Rappaport, E. Barbinis, D. Fleischman, A. Anabtawi, The structure of Titan's atmosphere from Cassini radio occultations: occultations from the prime and equinox missions. *Icarus* **221**, 1020–1031 (2012)
- E. Sciamma-O'Brien, N. Carrasco, C. Szopa, A. Buch, G. Cernogora, Titan's atmosphere: an optimal gas mixture for aerosol production? *Icarus* **209**, 704–714 (2010)
- S. Solomon, Stratospheric ozone depletion: a review of concepts and history. *Rev. Geophys.* **37**, 275–316 (1999)
- C. Sotin, K.J. Lawrence, B. Reinhardt, J.W. Barnes, R.H. Brown, A.G. Hayes, S. Le Mouélic, S. Rodriguez, J.M. Soderblom, L.A. Soderblom, K.H. Baines, B.J. Buratti, R.N. Clark, R. Jaumann, P.D. Nicholson, K. Stephan, Observations of Titan's northern lakes at 5 μm: implications for the organic cycle and geology. *Icarus* **221**, 768–786 (2012)
- E.R. Stofan, C. Elachi, J.I. Lunine, R.D. Lorenz, B. Stiles, K.L. Mitchell, S. Ostro, L. Soderblom, C. Wood, H. Zebker, S. Wall, M. Janssen, R. Kirk, R. Lopes, F. Paganelli, J. Radebaugh, L. Wye, Y. Anderson, M. Allison, R. Boehmer, P. Callahan, P. Encrenaz, E. Flamini, G. Francescetti, Y. Gim, G. Hamilton, S. Hensley, W.T.K. Johnson, K. Kelleher, D. Muhleman, P. Paillou, G. Picardi, F. Posa, L. Roth, R. Seu, S. Shaffer, S. Vetrella, R. West, The lakes of Titan. *Nature* **445**, 61–64 (2007)
- M. Sylvestre, N.A. Teanby, S. Vinatier, S. Lebonnois, P.G.J. Irwin, Seasonal evolution of C₂N₂, C₃H₄, and C₄H₂ abundances in Titan's lower stratosphere. *Astron. Astrophys.* **609**, A64 (2018)
- N.A. Teanby, P.G.J. Irwin, R. de Kok, S. Vinatier, B. Bézard, C.A. Nixon, F.M. Flasar, S.B. Calcutt, N.E. Bowles, L. Fletcher, C. Howett, F.W. Taylor, Vertical profiles of HCN, HC₃N, and C₂H₂ in Titan's atmosphere derived from Cassini/CIRS data. *Icarus* **186**, 364–384 (2007)
- N.A. Teanby, P.G.J. Irwin, C.A. Nixon, R. de Kok, S. Vinatier, A. Coustenis, E. Sefton-Nash, S.B. Calcutt, F.M. Flasar, Active upper-atmosphere chemistry and dynamics from polar circulation reversal on Titan. *Nature* **491**, 732–735 (2012)
- N.A. Teanby, B. Bézard, S. Vinatier, M. Sylvestre, C.A. Nixon, P.G.J. Irwin, R.J. de Kok, S.B. Calcutt, F.M. Flasar, The formation and evolution of Titan's winter polar vortex. *Nat. Commun.* **8**, 1586 (2017)
- M.G. Tomasko, Preliminary results of polarimetry and photometry of Titan at large phase angles from Pioneer 11. *J. Geophys. Res.* **85**, 5937–5942 (1980)
- M.G. Tomasko, P.H. Smith, Photometry and polarimetry of Titan—Pioneer 11 observations and their implications for aerosol properties. *Icarus* **51**, 65–95 (1982)
- M.G. Tomasko, L.R. Doose, L.E. Dafoe, C. See, Limits on the size of aerosols from measurements of linear polarization in Titan's atmosphere. *Icarus* **204**, 271–283 (2009)
- E.P. Turtle, A.D. Del Genio, J.M. Barbara, J.E. Perry, E.L. Schaller, A.S. McEwen, R.A. West, T.L. Ray, Seasonal changes in Titan's meteorology. *Geophys. Res. Lett.* **38**, L03203 (2011a)
- E.P. Turtle, J.E. Perry, A.G. Hayes, R.D. Lorenz, J.W. Barnes, A.S. McEwen, R.A. West, A.D. Del Genio, J.M. Barbara, J.I. Lunine, E.L. Schaller, T.L. Ray, R.M.C. Lopes, E.R. Stofan, Rapid and extensive surface changes near Titan's equator: evidence of April showers. *Science* **331**, 1414 (2011b)
- J. Veverka, Titan: polarimetric evidence for an optically thick atmosphere? *Icarus* **18**, 657–660 (1973)
- S. Vinatier, B. Bézard, C.A. Nixon, A. Mamoutkine, R.C. Carlson, D.E. Jennings, E.A. Guandique, N.A. Teanby, G.L. Bjoraker, F.M. Flasar, V.G. Kunde, Analysis of Cassini/CIRS limb spectra of Titan acquired during the nominal mission I. Hydrocarbons, nitriles and CO₂ vertical mixing ratio profiles. *Icarus* **205**, 559–570 (2010)
- S. Vinatier, B. Bézard, S. Lebonnois, N.A. Teanby, R.K. Achterberg, N. Gorius, A. Mamoutkine, E. Guandique, A. Jolly, D.E. Jennings, F.M. Flasar, Seasonal variations in Titan's middle atmosphere during the northern spring derived from Cassini/CIRS observations. *Icarus* **250**, 95–115 (2015)

- S. Vinatier, B. Schmitt, B. Bézard, P. Rannou, C. Dauphin, R. de Kok, D.E. Jennings, F.M. Flasar, Study of Titan's fall southern stratospheric polar cloud composition with Cassini/CIRS: detection of benzene ice. *Icarus* **310**, 89–104 (2018)
- J.H. Waite, W.S. Lewis, W.T. Kasprzak, V.G. Anicich, B.P. Block, T.E. Cravens, G.G. Fletcher, W.H. Ip, J.G. Luhmann, R.L. McNutt, H.B. Niemann, J.K. Parejko, J.E. Richards, R.L. Thorpe, E.M. Walter, R.V. Yelle, The Cassini Ion and Neutral Mass Spectrometer (INMS) investigation. *Space Sci. Rev.* **114**, 113–231 (2004)
- J.H. Waite, D.T. Young, T.E. Cravens, A.J. Coates, F.J. Crary, B. Magee, J. Westlake, The process of tholin formation in Titan's upper atmosphere. *Science* **316**, 870 (2007)
- R.A. West, A.D. Del Genio, J.M. Barbara, D. Toledo, P. Lavvas, P. Rannou, E.P. Turtle, J. Perry, Cassini imaging science subsystem observations of Titan's South polar cloud. *Icarus* **270**, 399–408 (2016)
- Y.L. Yung, M. Allen, J.P. Pinto, Photochemistry of the atmosphere of Titan—comparison between model and observations. *Astrophys. J. Suppl. Ser.* **55**, 465–506 (1984)